NYO-1480-116

Courant Institute of
Mathematical Sciences

AEC Computing and Applied Mathematics Center

A Finite Difference Method for the Solution of Free Boundary Problems

Eugene Bloch

AEC Research and Development Report

Mathematics and Computers
May 1969

New York University

UNCLASSIFIED

AEC Computing and Applied Mathematics Center
Courant Institute of Mathematical Sciences
New York University

Mathematics and Computers NYO-1480-116

A FINITE DIFFERENCE METHOD FOR THE SOLUTION OF FREE BOUNDARY PROBLEMS

Eugene Bloch

Contract No. AT(30-1)-1480

UNCLASSIFIED

Table of Contents

Abstract

A systematic iterative procedure is described which yields finite difference solutions to steady free boundary problems of plasma physics and fluid dynamics. By application of the method of steepest descent to minimize certain energy functionals connected with conformal mapping and free boundary problems, a system of artificially time-dependent equations is produced which converges to a steady state as the time parameter goes to infinity. The solution is obtained in a parametric form in which the physical plane is the conformal image of a fixed rectangle. The use of a fixed rectangle as the parameter domain enables us to treat effectively the difficulties engendered by the singular behavior of the stream function at the point of separation between the fixed and free boundaries. As a result the scheme can be made convergent to second order in the mesh width h.

The method has been applied successfully to the vena contracta and Riabouchinsky models of classical hydrodynamics for both plane and axially symmetric geometries. An accuracy of four significant figures in the calculation of quantities of physical interest can be obtained without difficulty. A plane equilibrium model of plasma physics is also computed. The scheme can be applied to a variety of problems with two independent variables.

1. INTRODUCTION

Free boundary problems are among the most difficult to treat either analytically or numerically. Examples of such problems are found in the occurrence of jets or cavities in classical hydrodynamics, where the location of a portion Γ of the boundary is unknown. These problems can be formulated in terms of a stream function ψ which is the solution of a Dirichlet problem in the flow region of the physical plane. The additional free boundary condition

$$q = \text{constant}$$

is specified on the free boundary Γ, where q is the speed of the fluid. This condition, which is motivated physically by Bernouilli's Law, compensates for the fact that Γ is not known. In the case of plane flow, where function theory can be applied, the solution in certain cases can be found analytically by the hodograph method. For three dimensional flows, for example those with axial symmetry, solutions to familiar models are not known, although existence and uniqueness theorems have been established. Other instances of free boundary problems which are of great interest arise in plasma physics. The equilibrium state of a perfectly conducting fluid contained by a magnetic field is an example, where the free boundary is determined by the balance between hydrodynamic and magnetic pressure.

The subject of this paper is the formulation and implementation of a finite difference method for treating these problems which is both stable and consistent. There are two difficulties which must be overcome in such an approach:

1) It can be shown quite generally that the stream function possesses singular behavior at the separation point z_o between the free boundary Γ and the fixed boundary Γ_F of the flow region. More precisely, the stream function has a regular expansion there in terms of the square root $(z-z_o)^{1/2}$, where z is the complex variable $x+iy$ in the physical plane. If z is used as the independent variable, then this behavior is an inherent source of high truncation error in the discrete solution.

2) Provision must be made for the determination of the free boundary by some systematic iterative procedure. Again, if the physical plane is used as the domain of the independent variable, there are difficulties associated with the implementation of any iterative technique caused by the changing geometry of the flow region.

The method we shall describe is designed to deal with both of these difficulties and can be applied to a variety of problems involving only two independent variables. We establish a parametric formulation by introducing a fixed rectangle R in an auxiliary w-plane. We seek the stream function as the solution to an appropriate Dirichlet problem

in R, and we seek the flow region as the image of R by a conformal mapping $z = z(w)$. We can set up the boundary correspondences for this mapping so that a corner of the rectangle is mapped into the separation point. When this is done, the difficulties caused by singular behavior are removed because both ψ and z become regular functions of w at the separation point. The required conformal mapping is obtained by solving an artificially time-dependent system of equations which converge to a steady state. This system of equations is derived by applying the method of steepest descent to minimize certain energy functionals connected with conformal mapping and free boundary problems. Steady state is achieved under conditions which guarantee that the mapping is conformal if and only if the free boundary condition is satisfied on Γ. The difficulty of locating the free boundary is automatically eliminated because we solve all equations in the fixed rectangle R.

It should be emphasized that since we have uniformized the singularity at the separation point in this formulation, we expect the over-all finite difference method to converge to the continuous solution as the mesh width $h \to 0$. Furthermore, since all equations are solved in a rectangle, it becomes a particularly simple task to write finite difference analogs which are accurate to second order in h. Therefore the convergence is $O(h^2)$. One of the objects of our numerical calculations is to verify this behavior by using a sufficiently large number of mesh points. Our use of conformal mapping is

quite essential because it assures that the equation for the stream function, when written in a conformally invariant form, makes sense in the rectangle. This conformal invariance is obvious in the case of plane flows, but it exists also, for example, in the case of axially symmetric flows when the governing equation is written in the form

$$\Delta\psi - (\nabla y \cdot \nabla\psi)/y = 0 \ .$$

In general, the modification of the scheme to deal with any example in two independent variables whose differential equation is conformally invariant is a relatively easy matter.

The central issue in this method is not the solution of the equation for ψ, as it is in the direct approach, but the establishment of the appropriate flow region as the conformal image of the rectangle. In achieving this mapping the stream function enters only in the determination of the speed along the free boundary. For example, in axially symmetric flows, the speed along any streamline is given by

$$q = |\nabla\psi|/y \ ,$$

and a conformal mapping is sought for which this quantity is constant along Γ. We include calculations of axially symmetric flows in our sample problems to demonstrate the applicability of the method in these cases.

In Section 2 we describe the particular models which were studied as examples. These are the vena contracta and Riabouchinsky models of classical hydrodynamics for both plane and axially symmetric geometries, and a simplified plane equilibrium model of plasma physics, which provided a pilot case on which the method was tested. We also give details relative to the calculations which were made for these models, and a brief review of previous research effort. Section 3 contains the derivation of the method. In Section 4 details of the application of the method to each of the models are described, as well as the general numerical formulation. The bulk of the research work was done here, for there are several subtle considerations which arise in connection with the problem of mapping the corner of R into the separation point. In Section 5 we give the results of the computations. Our fundamental conclusion is that the method can be applied successfully to the models we studied, although in some cases convergence is a delicate matter. Beyond this we verify that the convergence is $O(h^2)$ and we demonstrate the accuracy attainable by calculating contraction coefficients and drag coefficients to four significant figures. Also, a few fragmentary results are presented pertinent to the use of our method as a technique for conformal mapping per se. Appendix B comprises the FØRTRAN IV coded program for both the plane and axially symmetric Riabouchinsky models, as written for the CDC 6600 computer at New York University.

2. FREE BOUNDARY MODELS

We describe the three mathematical models to which our numerical method was applied. In each case a brief description of the physical problem is given, the equations of steady flow are formulated, and analytic solutions, where known, are given. For the vena contracta model, an asymptotic analysis of the behavior of the jet is also described, to provide a theoretical basis for certain extrapolations used in calculating contraction coefficients. We close with a brief discussion of some of the previous research on these problems and the difficulties inherent in a finite difference approach.

2.1. Cusped Geometry Model

Our purpose in studying this model is that it provides an elementary example with which to exhibit the numerical technique to be described. It incorporates some, but not all, of the features of the method. The cusped geometry model is of importance in plasma physics as a simplified plane mathematical model of the equilibrium state of a perfectly conducting fluid contained by a magnetic field [1].

The fluid is located in a doubly periodic array of cusped figures of equilibrium with boundaries Γ, whose cross-sections are shown in Figure 2.1. Their centers lie at the lattice points $(n+in')\ell$ (n and n' odd). A magnetic field B is generated by currents which flow in alternate directions along circular coils of radius r and boundary Ω which are also

periodically arranged at the points $(n+in')\ell$ (n and n' even). In the vacuum region D between Γ and Ω, the field B satisfies the Maxwell equations

$$\nabla \times B = 0$$

$$\nabla \cdot B = 0$$

with the associated boundary condition

$$B \cdot \nu = 0$$

on Ω and Γ. Since the vector B lies in the (x,y)-plane we can introduce a scalar magnetic potential ψ defined by

$$B = \nabla \times (0,0,\psi)$$

and formulate the problem for ψ, after introducing an appropriate normalization, as

$$\Delta\psi = 0$$

in D,

$$\psi = 0$$

on Γ, and

$$\psi = \pm 1$$

on the boundary Ω of alternate coils. The balance between magnetic forces and the hydrodynamic pressure in the fluid gives the additional free boundary condition

$$B^2 = (\nabla\psi)^2 = \text{constant}$$

which holds on Γ.

The uniqueness of the solution and the stability of these cusped figures of equilibrium can be established by showing that the energy of the system is a minimum relative to all configurations with the same total mass of fluid [1].

For our numerical method, it is convenient to formulate this problem in a different way. Considerations of symmetry permit us to confine our attention to the determination of ψ in the fundamental region D_z bounded by the lines $x = \pm\ell$, $y = \pm\ell$ and the corresponding parts of Γ, as shown in Figure 2.1. By symmetry, we have

$$\psi = 0$$

along these lines. We introduce a fixed rectangle R in the first quadrant of an auxiliary w-plane, where $w = u + iv$. The rectangle is bounded by the coordinate axes and the lines $u = a$, $v = b$. We seek the solution parametrically in terms of the variable w in R. The mapping from R to D_z is to be a conformal transformation, periodic in u, in which the boundary $v = b$ maps onto Ω, the boundary $v = 0$ maps onto the outer boundary of D_z, and the vertical boundaries $u = 0$, $u = a$ map onto the segment $y = 0$, $r \leq x \leq \ell$. With these boundary correspondences, the parametric solution for ψ is given by

$$\psi = v/b$$

when the boundary conditions on ∂D_z are transferred to the boundary of R. Apart from the factor b, we observe that R is the domain of a complex potential of which ψ is the imaginary part. Our original problem is therefore inverted, and becomes the determination of the unique conformal mapping of R onto D_z, with the indicated boundary correspondences, for which the boundary Γ is located so that the free boundary condition holds along it. Relative to the w-plane, the free boundary condition takes the form

$$|\nabla_z \psi|^2 = \psi_v^2/(x_v^2 + y_v^2) = \text{constant} .$$

The technique for achieving this conformal mapping is the basis of the numerical method and is described in Section 3.

2.2. Riabouchinsky Model

This hydrodynamic model is a representation of steady potential flow past an obstacle C in which cavitation occurs [2]. The cavity volume is kept finite by the introduction of a fictitious image obstacle C^* located downstream from C. We study this flow in both plane and axially symmetric geometries for the configuration shown in Figure 2.2.

A uniform stream directed along the positive x-axis and of speed U impinges on the obstacle C. A cavity of water vapor is formed behind C, bounded by the free streamlines Γ and Γ^* which detach from C and join the image obstacle C^* at the points indicated. The coordinates are placed so that

symmetry is achieved in both the x- and y-axes. In the plane case these coordinates lie in a cross-section of the flow and the obstacle is an infinite flat plate whose cross-section C has length $2y_o$. In the axially symmetric case, Figure 2.2 depicts a meridian plane, and the obstacle is a flat circular plate of radius y_o. The flow for both geometries can be described in terms of a stream function $\psi = \psi(x,y)$, defined in the region D exterior to the cavity, from which the velocity components of a fluid particle are found by the equations

$$V_x = \psi_y / y^m$$

(1)

$$V_y = -\psi_x / y^m$$

where $m = 0$ in the plane case and $m = 1$ in the axially symmetric case. From (1) we derive the relation for the speed q along any streamline ψ = constant, as

$$q = |\nabla_z \psi| / y^m = \psi_n / y^m \tag{2}$$

where n is the normal to the streamline in the usual sense, and ∇_z denotes the gradient in the z-plane, $z = x + iy$. The free streamlines Γ and Γ^* are unknowns and must be determined as part of the solution. The cavity is a domain of constant vapor pressure, and for stability of the flow we expect a continuous variation of pressure across the free streamlines. Therefore, an application of Bernouilli's law yields the free boundary condition

$$q = q_o = \text{constant}$$

along Γ and Γ^*. We define the cavitation parameter σ by the formula

$$\sigma = (q_o^2 - U^2)/U^2 \ .$$

The significance of σ is that specification of its value fixes the shape of the cavity, apart from a multiplicative factor which scales the size of the physical domain D.

Using symmetry, we consider the flow in the subdomain D_z of D in the first quadrant of the z-plane. We have the following problem for the determination of ψ:

(3a) $$\Delta\psi - (m/y)\cdot\psi_y = 0 \quad \text{in } D_z \ .$$

(3b) $$\psi = 0 \quad \text{on} \quad \Gamma + C^* + \text{x-axis} \ ,$$

(3c) $$\psi_x = 0$$

on the y-axis above the free streamline, by symmetry,

(3d) $$q = q_o \quad \text{on } \Gamma \ ,$$

(3e) $$\psi \sim U/(1+m)\cdot y^{1+m} \quad \text{as} \quad |z| \to \infty \ .$$

The asymptotic behavior (3e) is consistent with the assumption of a uniform stream at ∞.

In the plane model, where we have the tool of function theory, the solution can be found analytically by the hodograph method [2], in terms of the complex potential $\zeta = \phi + i\psi$, as the conformal mapping

$$(4)\quad z(\zeta) = \frac{1}{q_o}\left[\alpha^2(\zeta^2-1)^{1/2} + (1+\alpha^2)^{1/2}/\alpha \cdot \int_0^{\zeta} \left(\frac{\zeta^2 - \frac{1}{1+\alpha^2}}{\zeta^2 - 1}\right)^{1/2} d\zeta \right.$$

$$\left. + \frac{i}{\alpha} \int_{1/(1+\alpha^2)^{1/2}}^{1} \left(\frac{\zeta^2 - \frac{1}{1+\alpha^2}}{1 - \zeta^2}\right)^{1/2} d\zeta \right]$$

where the quantity α is defined by

$$\alpha = \frac{1}{2}\,(q_o^2 - U^2)/q_o U$$

and the ζ-plane has been normalized so that $\zeta = 1$ at the stagnation point B. The domains D_ζ and D_z relative to (4) are shown in Figure 2.3a and 2.3b.

For the axially symmetric case, the analytic solution is not known. Existence and uniqueness proofs have been established for a wide variety of such axially symmetric flows by use of variational principles [3].

It is necessary, for our numerical technique, to express the plane solution in a certain parametric form. We choose to normalize the flow so that $q_o = 1$, and we define the parameter k by

$$k = (1+\alpha^2)^{-1/2} \ .$$

We introduce a rectangle R in a w-plane, $w = u + iv$, oriented as shown in Figure 2.3c, and observe that the transformation

$$\zeta = k.sn(w,k) \tag{5}$$

maps R onto D_ζ [4]. The ratio K'/K is determined uniquely by k, and the scaling is chosen so that the boundary correspondences are as shown. In this context, the parameter k is the modulus of the Jacobian elliptic function sn. Substitution of (5) into the mapping (4), and use of the normalization we have indicated, gives

$$z(w) = (1/k)[E(w,k) - k'^2 w + ik'dn(w,k) + i(E' - k^2K')] \ , \tag{6}$$

where $E(w,k)$ is the elliptic integral of the second kind, $E' = E(K',k')$, and k' is the complementary modulus defined by

$$k'^2 = 1 - k^2 \ .$$

The drag coefficient C_D, the cavitation parameter σ, and the speed at infinity U can be expressed in terms of k by the formulas

$$C_D = 2(1+\sigma)(E' - k^2K')/(k'^2 + E' - k^2K')$$

$$\sigma = 2k'/(1-k')$$

$$U = k/(1+k') \ .$$

These quantities, and equations (5) and (6), are used both to provide initial conditions for the numerical calculation and to check the accuracy of the finite difference solution in the plane case. We note that as the length-to-width ratio r of the rectangle increases, the parameter $k \to 1$. The model approaches classical Helmholtz flow [2] in which $\sigma \to 0$ and the cavity behind the plate becomes infinite. In the limiting case, we have

$$C_D = 2\pi/(\pi+4) \doteq .87980$$

$$U = 1 .$$

In our numerical calculations we shall estimate the drag coefficient for both plane and axially symmetric cases as $\sigma \to 0$. It should be observed that letting $r \to \infty$ is a poor way of approximating Helmholtz flow, for it is well known that the shape of the Helmholtz free boundary approaches a parabola at large distances from the plate.

2.3. Vena Contracta Model

This is a hydrodynamic model of steady potential flow of an incompressible fluid which issues from an orifice in a plane wall [2]. The geometry is shown in Figure 2.4 for both plane and axially symmetric geometries. The physical coordinates x and y define a cross-section of the flow in the plane case and the orifice is an infinite slit of width $2y_o$. In the axially symmetric case, these coordinates depict a meridian plane and

the orifice is to be interpreted as a circular hole of radius y_o.

A jet of fluid issues horizontally from the orifice, to the left of which lies an infinite reservoir of fluid. The flow can be characterized in both geometries by a stream function $\psi = \psi(x,y)$ from which the velocity components and the speed are given by equations (1) and (2). The x-axis is a line of symmetry so that the flow region D_z is bounded by the x-axis, by the vertical wall $y \geq y_o$ and by the free streamline Γ which detaches from the wall at the separation point $z_o = iy_o$ and is asymptotic to the line $y = y_\infty$ as $x \to +\infty$. Along this free boundary, whose location must be found as part of the solution, continuity of the pressure and an application of Bernouilli's law gives the condition that the fluid speed there is constant. Thus we have the following problem for the determination of ψ:

(7a) $$\Delta\psi - (m/y)\cdot\psi_y = 0 \quad \text{in } D_z \ ,$$

where $m = 0$ in the plane case and $m = 1$ in the axially symmetric case,

(7b) $$\psi = 0 \quad \text{on x-axis} \ ,$$

(7c) $$\psi = C$$

on $y \geq y_o$ and on Γ, where $C \neq 0$ is a constant, and

(7d) $$q = q_o \quad \text{on } \Gamma \ ,$$

where q_o is the constant speed. Far downstream in the jet the flow becomes uniform, so that ψ has the asymptotic form

$$\psi \sim q_o y^{1+m}/(1+m) \quad \text{as } x \to +\infty \tag{7e}$$

in terms of the speed q_o. The constant C in (7c) is related to the other parameters by

$$C = q_o y_\infty^{1+m}/(1+m) .$$

The quantitative measure of the vena contracta (the narrowing of the jet as $x \to +\infty$) is the contraction coefficient C_m defined as the ratio of the cross-sectional area of the jet at $x = +\infty$ to its area at the orifice. For the geometries we study this definition takes the form

$$C_m = (y_\infty / y_o)^{1+m} .$$

In the plane case the flow can be found analytically by the hodograph method in terms of the complex potential $\zeta = \phi + i\psi$. Introducing the normalization $C = 1$, we obtain the solution as the conformal map of the strip $0 \leq \text{Im } \zeta \leq 1$ onto D_z given by

$$z(\zeta) = -(2C_o y_o/\pi)\left[e^{-\zeta\pi/2} + (1 + e^{-\pi\zeta})^{1/2} + \log\left(e^{\zeta\pi/2}[(1+e^{-\pi\zeta})^{1/2} - 1]\right)\right] , \tag{8}$$

with boundary correspondences arranged so that

$$z(i) = y_o$$

$$z(+\infty) = +\infty$$

$$z(-\infty) = -\infty \ .$$

By substitution of $\zeta = i$ into (8), the contraction coefficient is found to be

$$C_o = \pi/(\pi+2) \ .$$

The analytic solution for the axially symmetric vena contracta is not known.

For our numerical approach it is necessary to consider a modified vena contracta model, in order to conveniently obtain a parametric formulation in which the physical plane is a conformal mapping from a fixed rectangle R in an auxiliary w-plane. To achieve this modification, we truncate the infinite jet at a distance ℓ downstream from the fixed wall, and impose the boundary condition

(7e') $$\psi_x/y^m = 0$$

along $x = \ell$, which means physically that the velocity vector there is horizontal. All other conditions (7a-7d) remain the same. This modification is tantamount to the assumption of an image reservoir of fluid, at distance 2ℓ downstream, back into which the fluid flows. In this respect the truncated vena contracta model is quite similar to the Riabouchinsky model.

We conjecture that the flow corresponding to the truncated jet problem converges to the infinite jet flow in any fixed bounded subdomain of D_z to the left of $x = \ell$ as $\ell \to \infty$. In particular, we define the truncated jet contraction coefficient $C_m(\ell)$ to be the ratio of the cross-sectional area of the jet at $x = \ell$ to its area at the orifice, and we assert that the asymptotic behavior of $C_m(\ell)$ is given by

$$C_m(\ell) \sim C_m + A_m e^{-\lambda_m \ell} \quad \text{as } \ell \to \infty \tag{9}$$

in both plane ($m = 0$) and axially symmetric ($m = 1$) geometries, for appropriate values of the constants A_m and λ_m. Let $z = z(w)$ be the analytic function we seek which maps the rectangle R in the w-plane onto the domain D_z. Assume this mapping is arranged so that the boundary correspondences are as shown in Figure 2.5, and is normalized so that the jet height at $x = \ell$ is 1. Then for large ℓ the transformation has the form

$$z(w) = \alpha_1 + \alpha_2 w + z_\ell(w) ,$$

where α_1 and α_2 are real constants and $z_\ell(w) \to 0$ as $\mathrm{Re}\,(w) \to a$; that is, the mapping is approximately affine near the edge BC. From this observation we conclude that ℓ satisfies the approximate formula

$$\ell = \alpha_1 + r ,$$

where r is the length-width ratio of R. Therefore the asymptotic formula (9) is equivalent to

$$C_m(r) \sim C_m + A_m e^{-\lambda_m r} \quad \text{as } r \to \infty \tag{10}$$

for some constants A_m and λ_m.

In what follows we aim first to directly verify (10) in the plane case and second to obtain estimates for the values of λ_m for both the plane and axially symmetric models. Our purpose in doing this is to provide a check on the estimation of C_m by our numerical method. In the plane case, the truncated model can be solved completely by the hodograph method. From this solution the contraction coefficient can be calculated directly as

$$C_o(r) = (k' + E')/(1 + E')$$

where k' is the complementary modulus of the elliptic functions and integrals associated with the rectangle R, and E' is the complete elliptic integral of the second kind with respect to k'. This integral is even in k' and has the expansion [4]

$$E' = \pi/2 + O(k'^2)$$

The parameter k' is related to r by the formula [4]

$$k' = e^{-r\pi/2} + O(e^{-\pi r})$$

for large r. Therefore we obtain

$$C_o(r) \sim \pi/(\pi+2) + A_o e^{-r\pi/2} , \quad \text{as } r \to \infty$$

which verifies (10) and gives

$$\lambda_o = \pi/2$$

for the plane case.

For the axially symmetric case, where we have no rigorous analysis, we can show that the asymptotic behavior of the free streamline for the infinite jet model, where y_∞ is normalized to be 1, is given by

$$y(x) \sim 1 + A_1 e^{-\lambda_1 x} , \quad x \to \infty \tag{11}$$

with an estimate on the value of λ_1 which appears in the exponent. We make the further conjecture that this value of λ_1 is the same constant which appears in (10). To prove (11), we observe that by (7e) the stream function for the infinite jet model has the form

$$\psi = y^2/2 + \psi_1(x,y) \tag{12}$$

where $\psi_1 \to 0$ as $x \to +\infty$, and where we have adopted the normalization $q_o = 1$. The function ψ satisfies

$$q_o = \psi_n/y = 1$$

$$\psi = 1/2$$

on the free boundary Γ, and therefore also the mixed condition

(13) $$\psi_n/y + (\kappa/y)(\psi - 1/2) = 1 ,$$

where κ is the curvature along Γ. Following an idea due to Garabedian [5], we observe that the condition that the flow is irrotational,

$$q_n + \kappa q = 0$$

which holds along any streamline, can be used to show that (13) is satisfied by ψ along an approximation Γ^* to Γ to second order in the normal displacement δn between Γ and Γ^*. We use this result to obtain an estimate for λ_1. Let the line $y = 1$ be the approximate free boundary Γ^*. We impose the boundary condition (13) on Γ^*, and use equation (12) and the fact that $\kappa = 0$ on Γ^* to obtain the condition

$$(\psi_1)_y = 0$$

on Γ^*. On the x-axis we have

$$\psi = \psi_1 = 0 ,$$

and throughout D_z, ψ_1 satisfies

$$\Delta\psi_1 - (\psi_1)_y/y = 0 \ .$$

Thus we have an eigenvalue problem for the determination of ψ_1, which is valid for large positive x. Using separation of variables we obtain the solutions

$$\psi_1 = Cye^{-\lambda x} \cdot J_o'(\lambda y) \ .$$

The smallest value of λ which satisfies the boundary conditions is the smallest solution to

$$J_o'(\lambda) + \lambda J_o''(\lambda) = -\lambda^2 J_o(\lambda) = 0 \ ,$$

from which we obtain

$$\lambda_1 \cong 2.4 \ .$$

Substituting ψ_1 into (12) and using the condition $\psi = 1/2$ on Γ gives an implicit equation for the free boundary

$$1/2 = y^2/2 + Ce^{-\lambda x} y \, J_o'(\lambda y) \ .$$

It is easy to show that for sufficiently large x this equation has the form (11), which is what we set out to prove. The same analysis can be carried out for the plane model. The result is $\lambda_o = \pi/2$ which agrees with the value obtained by the rigorous treatment. This supports our conjecture that the free boundary of the infinite jet and the truncated contraction coefficient

have quantitatively the same asymptotic behavior. We use these results in Section 4.3.7. We observe here that the value of the exponent λ_m is substantially larger in the axially symmetric case compared to the plane case. This suggests that the convergence to the infinite jet model as $\ell \to \infty$ is substantially faster in the axially symmetric case than in the plane case.

2.4. The Difficulties of Applying a Finite-Difference Method

For any of the models introduced there are two problems associated with using finite differences to solve directly for ψ as a function of the physical variables. First, the determination of the free boundary requires an iterative technique in which a trial free boundary is selected and then modified in the next iterative cycle to produce a better guess. Such schemes have been applied, with the corrections made essentially by trial and error, in [6] for the axially symmetric vena contracta, and in [7] for the plane and axially symmetric Riabouchinsky models. Corrections of a trial free boundary can be made automatically with the technique used in Section 2.3 for obtaining the asymptotic behavior of the vena contracta jet, and should produce a second order rate of convergence. This has been accomplished recently in [8], where the free boundary is approximated by choosing the multiplicative constants in a linear combination of appropriate functions. The second, and more serious, problem is that the separation point z_o is a singular point of the flow. For the plane models

the hodograph method shows that the stream function expansion near z_o is regular in powers of $(z-z_o)^{1/2}$, and the same type of behavior holds in the axially symmetric cases, as shown in [9]. In these expansions the first term is zero since the speed is finite at z_o, but in any case, the finite difference equations exhibit unbounded truncation error near z_o. In the papers [6] and [7] cited above, an attempt is made to deal with this difficulty by refinement of the mesh in the vicinity of z_o. Such procedures localize but do not remove the difficulty. The results of these calculations are not convincing. In the vena contracta model the free boundary makes an angle of almost 30^o with the vertical, whereas it is supposed to be 0^o. Also, comparison between computed and exact Riabouchinsky plane flows shows a wide discrepancy in the free boundary location. In [8] the effect of the singularity is reduced by incorporating into the linear combination functions which describe the singular behavior. This makes possible a better description of the free boundary near the separation point.

The method presented in this paper removes both of these difficulties in its application to the hydrodynamic models. We establish a systematic iterative procedure for the determination of Γ which is made independent of the changing geometry. We deal with the singular behavior by formulating the problem parametrically. The physical plane is sought as a conformal transformation from a fixed rectangle, one of whose corners is made to map onto the separation point. We describe this method in detail in Section 3.

3. THE METHOD OF STEEPEST DESCENT

3.1. General Description

The numerical method alters the formulation of a free boundary problem in the following way. We introduce a fixed rectangle R in an auxiliary w-plane and we seek the solution in the parametric form

$$\psi = \psi(w)$$

$$z = z(w) \ .$$

The function $z(w)$ is to be found as the analytic function which maps R onto the flow region. The free boundary Γ is to be determined along with this mapping. The function ψ 'solves a Dirichlet problem in R, provided that its governing equation is conformally invariant.

The possibility of implementing this approach rests on devising a technique for obtaining the conformal map. We couple two distinct variational principles, one for free boundary problems, and the other for the Plateau problem, which, by the application of the method of steepest descent, produce an artificially time-dependent system of equations whose steady state solutions yield the desired mapping.

3.2. Variational Principle — Conformal Mapping

We cite a result connected with the minimum formulation of the Plateau problem [10]. Let $\mathcal{C}$ be the class of differentiable functions $z(w) = x(u,v) + iy(u,v)$ which map the domain R

in the w-plane onto some fixed domain D in the z-plane, and which map the boundary ∂R onto the boundary ∂D in such a way that three specified points on ∂R go into three specified points on ∂D. The domain R is a rectangle in the first quadrant of the w-plane with horizontal and vertical sides. Then the conformal mapping between R and D is that function in $\mathcal{C}$ which minimizes the Dirichlet-Douglas integral

$$J = \frac{1}{2}\iint_R [(\nabla x)^2 + (\nabla y)^2]dudv \quad . \tag{1}$$

The three point condition in our hypothesis serves to make the mapping unique. The method of steepest descent can be applied to J in order to find this conformal mapping. We introduce t as an artificial time parameter and regard z as a function of t as well as w. Then J becomes a function of t which we want to decay as rapidly as possible as $t \to \infty$. To achieve this, we differentiate J with respect to t to obtain

$$\frac{dJ}{dt} = -\iint_R [\Delta x\ x_t + \Delta y\ y_t]dudv - \oint_{\partial R} (x_\nu x_t + y_\nu y_t)ds$$

where ν is the inner normal and s is the arc length on ∂R. Paths of steepest descent are those which assure that each of the integrands on the right is positive. Thus we are led to specify

$$x_t = \alpha \Delta x$$

$$y_t = \alpha \Delta y$$

in R, where the positive constant α is arbitrary. This factor controls the rate of convergence as $t \to \infty$ and has the usual interpretation in the steepest descent idea, namely that the method tells the "direction" in which to move, but not how far to move. On the boundary, the same considerations lead to the equation

$$x_t + iy_t = \beta[(x_\nu x_s + y_\nu y_s)/(x_s^2 + y_s^2)](x_s + iy_s) \ .$$

This boundary condition is consistent with the requirement that the boundary points of R go into boundary points of D. It has a simple geometric interpretation. The vector (x_s, y_s) is always tangential to ∂D, but the vector (x_ν, y_ν) will be normal to ∂D only when steady state $(x_\nu x_s + y_\nu y_s = 0)$ is reached. A boundary point is therefore shifted tangentially along ∂D at time 't by an amount proportional to the tangential component of (x_ν, y_ν). The factor β is a positive constant.

As $t \to \infty$ a steady state is reached in which we obtain

$$\Delta x = 0 \ , \quad \Delta y = 0 \tag{2}$$

in R, and

$$x_\nu x_s + y_\nu y_s = 0 \tag{3}$$

on ∂R. Since the rectangle R has horizontal and vertical sides the s and ν derivatives are equivalent to u and v derivatives, and so the boundary condition (3) implies

$$x_u x_v + y_u y_v = 0 \tag{4}$$

on ∂R. The function $x_u x_v + y_u y_v$ is harmonic in R, because x and y are themselves harmonic in the steady state, and so (4) actually holds throughout R. Moreover, using a familiar theorem from function theory, we obtain the result that the harmonic conjugate of this function is identically constant, that is,

$$x_v^2 + y_v^2 - x_u^2 - y_u^2 \equiv H \tag{5}$$

in R. In these terms, the assertion of the minimum principle is that $H \equiv 0$, from which we see that (4) and (5) together are equivalent to the Cauchy-Riemann conditions. The method of steepest descent therefore provides a technique for obtaining conformal mappings.

Suppose now that the requirements on the mapping are over-specified by having a four-point condition instead of the three-point condition described above. If for our models we envision fixed guesses for the free boundary locations, then we are dealing with such an over-specified problem. If the integral (1) possesses a minimum at all, then our analysis can be carried out just as above except that the constant H in (5) is not necessarily equal to zero. Thus we must modify the mapping procedure by building in a mechanism for moving the free boundary Γ around until in the steady state we have $H = 0$. There are, of course, many boundary locations for which this conformality condition is met. It is our aim to incorporate

a means by which that particular curve is singled out which also satisfies the free boundary condition. We achieve this by use of the variational principle described in the next section.

3.3. Variational Principle — Free Boundary Problems

We establish the free boundary by applying the method of steepest descent to the following variational principle associated with free boundary problems [3]. Among all admissible boundaries Γ^*, each of which defines a domain D_z^* in which we can find a stream function ψ which satisfies the Dirichlet conditions on the boundary, the appropriate free boundary Γ is characterized by the property that the energy M of the flow is a minimum for a fixed representative mass (or volume) V. This principle can be formulated as an isoperimetric problem in the calculus of variations in which we minimize the functional

$$J_F = M - \lambda^2 V$$

with respect to all admissible free boundary configurations. As a particular example, the appropriate expressions for M and V for the Riabouchinsky models can be shown to be

$$M = \pi^m \iint_D [\nabla(\psi - y^{1+m}/(1+m))]^2 y^m \, dxdy$$

$$V = (2\pi)^m \iint_\Omega y^m \, dxdy$$

where Ω represents the cavity [3]. If δn represents an

arbitrary perturbation of the free boundary along its inner normal then we can calculate the first variation of J_F to be

$$\delta J_F = \int_\Gamma [(\nabla\psi/y^m)^2 - \lambda^2]\delta n \, ds \ .$$

Thus we obtain as a necessary condition for J_F to be a minimum the requirement

$$(\nabla\psi/y^m)^2 = \lambda^2$$

which is the free boundary condition, and the Lagrange multiplier λ represents the constant speed q_o along Γ.

Applying the method of steepest descent as a technique for implementing the minimization of J_F, we are led to the formula

$$\frac{dM}{dt} - \lambda^2 \frac{dV}{dt} = \int_\Gamma [\nabla\psi/y^m)^2 - \lambda^2]n_t ds$$

where n_t is the speed of Γ in the direction of its inner normal, and we specify

$$n_t = -\gamma((\nabla\psi/y^m)^2 - \lambda^2) \tag{6}$$

as the path of steepest descent, where the positive number γ represents a convergence factor. This variational principle applied to the other models leads also to equation (6) as the path of steepest descent, although the particular expressions for M and V are different. Formula (6) is essentially the

recipe used for modifying the free boundary in [6] and [7], with λ chosen as the average of $|\nabla\psi/y^m|$ computed over the free boundary. In the present context, we see that there is a mathematical basis for expecting such a recipe to converge, since it comes from a variational principle.

3.4. Combined Iterative Method

We use the two variational principles we have described to produce the following basic iterative scheme. In the fixed rectangle R we solve

$$\text{(7a)} \qquad \begin{aligned} x_t &= \alpha\Delta x \\ y_t &= \alpha\Delta y \\ \psi_t &= \alpha[\Delta\psi - m/y(\nabla\psi\cdot\nabla y)] \end{aligned}$$

We remark that the time-dependent formulation of the equation for ψ can be motivated by an application of the method of steepest descent to Dirichlet's principle for ψ over the physical domain. Furthermore, the form taken by this equation for $m = 1$, the axially symmetric case, is to maintain invariance under the conformal transformation $z(w)$.

On the boundary of R we impose conditions dictated by the variational principles. Along those parts of ∂R which map into the fixed boundary of D, we have

$$\text{(7b)} \qquad x_t + iy_t = \beta[(x_\nu x_s + y_\nu y_s)/(x_s^2 + y_s^2)](x_s + iy_s)$$

where the s and ν subscripts are either u or v derivatives. Equation (7b) is the tangential shift motivated by the conformal mapping procedure. On the part of ∂R which maps into the free boundary we impose, in addition to the tangential shift, a normal shift based on equation (6). We arrange the boundary correspondences so that the base of the rectangle corresponds to the free boundary, hence s = u and ν = v, and we obtain

$$(7c) \quad x_t + iy_t = \beta[(x_u x_v + y_u y_v)/(x_u^2 + y_u^2)](x_u + iy_u) + \gamma[y^{2m}(x_v^2 + y_v^2)/\psi_v^2 - 1/\lambda^2](x_v + iy_v) .$$

The second term on the right in (7c) represents an implementation of equation (6), where we have used the transformation

$$(8) \quad (\nabla_z \psi)^2 = \psi_v^2/(x_v^2 + y_v^2) .$$

The gradient ∇_z is applied in the physical domain along Γ. This transformation is valid when the mapping z(w) is conformal and we could use u-derivatives as well in the denominator of (8). The parameter λ is a suitably chosen constant. The vector (x_v, y_v) is the approximate inner normal to Γ.

The boundary conditions for ψ are the Dirichlet conditions transferred to the boundary of R.

Assuming that a steady state is reached, we have

$$\Delta x = 0$$

$$\Delta y = 0$$

$$\Delta\psi - (m/y)\nabla\psi \cdot \nabla y = 0$$

in R,

(9a) $$x_u x_v + y_u y_v = 0$$

(9b) $$x_v^2 + y_v^2 = x_u^2 + y_u^2 + H$$

in R and on ∂R, and

(10) $$y^{2m}(x_v^2 + y_v^2)/\psi_v^2 = 1/\lambda^2 = \text{constant}$$

on that part of ∂R which maps into Γ. Using (8), we see that (10) expresses the fact that the free boundary condition is satisfied. We have yet to indicate how the requirement $H = 0$ is achieved. This depends upon the choice for λ. For example, in the cusped geometry model, (where $m = 0$) we are able to obtain convergence with the formula

$$1/\lambda^2 = [(x_u^2 + y_u^2)/\psi_v^2]_o$$

where the subscript denotes an average over the free boundary. To show that $H = 0$, we combine (10) with (9b) to obtain

$$1/\lambda^2 = H/\psi_v^2 + (x_u^2 + y_u^2)/\psi_v^2 .$$

Upon taking averages in this equation and using the form for λ we have chosen, we get

$$H = 0 .$$

For the hydrodynamic models, the situation is considerably more delicate as regards the choice of λ. We consider the necessary refinements, as well as other details of the method as applied to each model, in Section 4.

3.5. Remarks on the Method

1. We observe that the kind of systematic iterative procedure we have described differs sharply from previous work in that the free boundary Γ in our method is modified at each time step, consistent with the overall formulation of a time-dependent problem. In previous work, a succession of Dirichlet or linear mixed problems were solved completely with a fixed guess for the location of Γ. The free boundary was then modified by an appropriate application of the free boundary condition to produce a better guess.

2. We have considerable freedom in our formulation to choose the boundary correspondences for the conformal mapping. We take advantage of the right-angled corners of the rectangle by specifying that one of these corners map into the separation point between the free and fixed boundaries of the flow region. In this way, both z and ψ become regular functions of w at the corner and the difficulty caused by the singular behavior of ψ in the z-plane is removed. The finite difference analogs of

the time dependent equations can be made accurate to second order in mesh width h over the whole rectangle, and we expect the convergence to the continuous solution to be $O(h^2)$.

3. We discuss the application of the method to a completely trivial example for the purpose of providing a geometric interpretation of the ideas we have introduced.

Consider the problem of mapping the square S onto the rectangle shown in Figure 3.1, such that the four corners A, B, C and D of the square map into the corresponding four corners of the rectangle. It is obvious that if we want the mapping to be conformal then the value of α must be 1 and the only solution is the identity

$$z = w \ .$$

Thus we shall ultimately allow the boundary BC in the z-plane to translate horizontally, governed in its motion by the normal shift condition, but let us assume for now that this boundary is fixed at $x = \alpha$. The affine mapping

$$\begin{aligned} y &= v \\ x &= \alpha u \end{aligned} \tag{11}$$

is obtained as the steady state solution which minimizes the Dirichlet-Douglas integral. The functions x and y are harmonic and we obviously have

$$x_u x_v + y_u y_v = 0$$

$$x_v^2 + y_v^2 - x_u^2 - y_u^2 = 1-\alpha^2 = \text{constant}$$

in the square and on its boundary. We see that only if $\alpha = 1$ will the mapping be conformal.

The general theory of the Plateau problem asserts that minimal surfaces in three dimensions (x,y,s), where we use s as the third coordinate to avoid confusion with the complex variable z, satisfy the parametric equations

$$\Delta x = \Delta y = \Delta s = 0$$

in S, and

$$x_u x_v + y_u y_v + s_u s_v = 0$$

$$x_v^2 + y_v^2 + s_v^2 - x_u^2 - y_u^2 - s_u^2 = 0$$

on the boundary. In the present context, we may interpret the solution (11) as the projection onto the (x,y)-plane of a three-dimensional minimal surface, whose s-coordinate satisfies

$$s_u s_v = 0$$

(12)

$$s_u^2 - s_v^2 = 1-\alpha^2$$

on ∂S and

$$\Delta s = 0$$

in S. Suppose $\alpha > 1$. Then for s to be real we must have, from equations (12)

$$s_u = 0$$

$$s_v = (\alpha^2-1)^{1/2}$$

from which we obtain

$$s = (\alpha^2-1)^{1/2}v \ .$$

Thus the three-dimensional minimal surface is a square in the coordinate system (x,y,s) which is hinged along the x-axis and inclined in the s-direction an appropriate amount so that its length is α. Conversely, if $\alpha < 1$, we obtain

$$s = (1-\alpha^2)^{1/2}u \ ,$$

which gives (as the minimal surface) an inclined square of side 1 which is hinged along the y-axis. Thus the effect, geometrically, of the normal shift in our formulas is to determine that minimal surface in a one-parameter family of surfaces for which

$$s = 0 \ ,$$

in which case the mapping will be conformal. Assume that $1/\lambda^2$ is chosen to be the average of $x_u^2 + y_u^2$ over BC. If $\alpha > 1$, this normal shift drives the boundary BC inward, as we see by inspection of equation (3.7c). If $\alpha < 1$, BC is moved outward. Therefore we expect the combined iterative procedure to converge.

4. THE FINITE DIFFERENCE SCHEME

The basic numerical scheme described in Section 3 is applied to the cusped geometry model, and to the plane and axially symmetric vena contracta and Riabouchinsky models introduced in Section 2. The cusped geometry model was chosen for study because it provides a simple example on which to test the method. As we will describe in Section 4.2, the method is applied in this case as a systematic iterative procedure for determining the appropriate physical domain in which the plasma physics problem is solved. No attempt is made to give special treatment to the separation points. In the formulation of this model we allow points to shift back and forth between free and fixed boundaries as $t \to \infty$. As a result the over-all method possesses a high degree of stability and there are no inherent problems in obtaining convergence, although the accuracy is poor. For the hydrodynamics models we introduce the additional feature of mapping a corner of the parameter domain rectangle into the separation point for the purpose of eliminating the effects of the singular behavior of the stream function. As we describe in Section 4.3, this formulation requires procedures of a considerably more delicate nature to produce a convergent scheme. We study the plane models so that we can check our numerical computations against the known analytic solutions. The axially symmetric models are calculated to demonstrate that the method can be applied to examples that are governed by differential equations other than Laplace's equation in two

dimensions. We also obtain for these cases new estimates of certain parameters of physical importance for the models studied. These are the contraction coefficients for the vena contracta and the drag coefficient for the Riabouchinsky model.

4.1. General Features of the Numerical Method

4.1.1. Basic Algorithm

Finite difference equations are written to approximate the differential equations for x, y, and ψ in R and on its boundary. We observe that since the basic domain is a rectangle, it is a simple task to produce finite difference equations which are accurate to second order in mesh size. Furthermore, we can arrange the dimensions of the rectangle to have a rational length-to-width ratio so that the mesh spacing h is equal in both horizontal and vertical directions.

The solution is obtained by the following steps:

1. An initial mapping is established which sets up the boundary correspondences to conform closely with the conformal mapping we seek. An initial solution for ψ is also selected.

2. The interior mesh points are scanned and we move forward one time step Δt in the solution of equations (3.7a) for x, y, and ψ.

3. The tangential shift (3.7b) is applied to those points on ∂R which map onto the fixed boundary of ∂D, which relocates their positions on the fixed boundary at the next time step.

Where appropriate, higher order normal corrections are applied to keep these points on the fixed boundary.

4. The combined tangential and normal shift given by (3.7c) is applied along the free boundary.

5. A check for convergence is performed. We examine the interior residuals as well as the boundary terms

$$(x_u x_v + y_u y_v)/(x_u^2 + y_u^2)$$

and

$$y^{2m}(x_v^2 + y_v^2)/\psi_v^2 - 1/\lambda^2$$

to see if the maximum of their absolute values lies below some specified error E. If not, we go back to step 2. If so, then the iterative process is terminated.

4.1.2. Interior Equations

The method of steepest descent produces the heat equation (3.7a) to be solved in R as $t \to \infty$. The formulas which result from using a forward difference for the time derivative with time step $\Delta t = 4h^2$, where h is the mesh width, correspond to the familiar Jacoby iterative method for Laplace's equation. This method is far too slow to be practical. Therefore, we use successive point over-relaxation, which yields the basic difference equation

$$(1) \quad x_{m,n}^{j+1} = (1-\omega)x_{m,n}^{j} + \omega(x_{m+1,n}^{j} + x_{m,n+1}^{j} + x_{m-1,n}^{j+1} + x_{m,n-1}^{j+1})/4$$

where ω is the relaxation factor and j denotes the time step.

Identical equations are used for y and for ψ in the plane case. The axially symmetric difference equation for ψ will be derived in Section 4.1.3. As $t \to \infty$ we obtain a finite-difference solution accurate to second order in h.

To conform to our point of view that the method specifies a time-dependent problem which approaches a steady state, we note that the over-relaxation formula (1) has an interpretation as the numerical analog of the hyperbolic equation [11],

$$x_{ut} - x_{vt} + \alpha x_t = \Delta x \ , \tag{2}$$

where the time step Δt in the finite difference analog is taken equal to h. The constant α, which we may interpret as a dissipation parameter, is related to the relaxation factor ω by the formula

$$\omega = 2/(1+\alpha h) \ . \tag{3}$$

Fourier analysis [11] can be applied to show that the finite difference solution to (2) approaches a steady state according to the estimate

$$|x^{\infty}_{m,n} - x^{N}_{m,n}| \leq Ae^{-\lambda Nh} \ , \tag{4}$$

where N is the total number of iterations, A and λ are numbers which depend only on α, and $x^{N}_{m,n}$ is the N^{th} iterated solution. This formula shows that the number of iterations required to achieve a specified accuracy grows like 1/h provided that the

relaxation factor is adjusted in accordance with formula (3) to maintain a constant α. The convergence rate indicated by (4) is in sharp contrast to that which is obtained by the Jacoby scheme. There, the number of iterations grows like $1/h^2$ [1]. In the present context the improvement provided by over-relaxation is due to the fact, indicated above, that we can take $\Delta t = h$ in the numerical analog of equation (2).

4.1.3. The Axially Symmetric ψ Equation

In the axially symmetric models the stream function satisfies the equation

$$\Delta_z \psi - \psi_y / y = 0 \tag{5}$$

in the z-plane. Invariance under a conformal transformation $z = z(w)$ is obtained when this equation is written in the form

$$\Delta \psi - (\nabla y \cdot \nabla \psi)/y = 0 \ . \tag{6}$$

Thus we may regard ψ and y in equation (6) as functions of w, with the operators Δ and ∇ acting in the w-plane. We seek ψ as a function of w over the rectangle R in our parametric formulation. As shown below, we can write finite difference equations for (6), which are accurate to second order in mesh size and which are suitable for solution by over-relaxation. However, for both hydrodynamic models, the conformal mapping we seek between R and the physical plane has a pole at a corner of R. In the neighborhood of this pole the truncation error in the finite difference approximation to (6) becomes unbounded.

We can remove this difficulty by use of the Kelvin inversion [12]

$$\psi^*(X,Y) = |Z|\psi(x,y) ,$$

where

$$Z = X + iY = 1/z$$

and

$$|Z|^2 = X^2 + Y^2 = 1/(x^2 + y^2) .$$

If ψ satisfies equation (5), then ψ^* satisfies

$$\Delta_Z \psi^* - \psi^*_Y/Y = 0 ,$$

or, in the w-plane

$$\Delta\psi^* - \nabla Y \cdot \nabla\psi^*/Y = 0 . \tag{7}$$

The transformation

$$Z = 1/z$$

maps the neighborhood of infinity in the z-plane onto a neighborhood of the origin in the Z-plane, and equation (7) can therefore be used instead of equation (6) in the vicinity of the pole.

Finite difference equations for either (6) or (7) which are accurate to second order in h can be obtained following the procedure in [7]. We write the differential equation in divergence form

$$y[\frac{\partial}{\partial u}(\psi_u/y) + \frac{\partial}{\partial v}(\psi_v/y)] = 0 .$$

Let the points in a grid of uniform mesh of width h be numbered as shown in Figure 4.1. A central difference on the outer u-derivative gives the expression

$$y_o[(\psi_u/y)_a - (\psi_u/y)_b]/2(h/2)$$

for the derivative at the point 0. If we use central differences on ψ_u at the points a and b and simple averages for y at a and b relative to the points 0, 1 and 3, 0 respectively, we obtain the formula

$$(8) \quad A = 2y_o/h^2\left[(\psi_1-\psi_o)/(y_1+y_o) - (\psi_o-\psi_3)/(y_3+y_o)\right]$$

as an approximation to $y\frac{\partial}{\partial u}(\psi_u/y)$ at the point 0. To see that it is accurate to second order in h, we note that A considered as a function of h has the expansion

$$A = A_o + A_1h + A_2h^2 + \ldots .$$

Since the quantities ψ and y satisfy

$$\psi_3(h) = \psi_1(-h)$$

$$y_3(h) = y_1(-h) ,$$

we conclude by inspection of the terms which appear in equation (8) that A is an even function of h. In particular,

$$A_1 = 0 \ .$$

Direct computation using Taylor series expansions shows that

$$A_o = (\psi_{uu} - y_u\psi_u/y)_o$$

and so A is a finite difference approximation accurate to $O(h^2)$.

Taking also the v-derivative into account, the finite difference equation for ψ at the point 0 is

$$(2y_o/h^2)\sum_{i=1}^{4} (\psi_i-\psi_o)/(y_i+y_o) = 0 \ .$$

We solve this equation for ψ_o, to obtain the form

$$\psi_o = \sum_{i=1}^{4} (a_i/a_o)\psi_i$$

where

$$a_i = (y_i+y_o)^{-1} \ , \qquad i = 1,2,3,4,$$

and

$$a_o = \sum_{i=1}^{4} a_i \ ,$$

which exhibits the strict diagonal dominance of the matrix for ψ. This matrix is also symmetric and therefore the system of equations is suitable for solution by successive over-relaxation. There are no difficulties associated with the circumstance of solving near y = 0.

4.1.4. Boundary Conditions

All space derivatives at the boundary of R are calculated to second order in h, using a central difference for the tangential derivatives and a 3-point formula for the normal derivatives. These formulas are given below relative to Figure 4.2, which shows appropriately labelled points in a grid of mesh width h.

$$\left.\frac{\partial f}{\partial \nu}\right|_1 = -(4f_1 - 3f_2 + f_3)/2h + O(h^2) , \tag{9a}$$

$$\left.\frac{\partial f}{\partial s}\right|_1 = (f_4 - f_5)/2h + O(h^2) . \tag{9b}$$

The quantity f stands for x, y or ψ. These derivatives are used to calculate the right-hand sides of the boundary equations (3.7b) and (3.7c). For the time derivatives in these boundary equations we use simple forward differences and we take the time step Δt equal to h. Thus we obtain difference equations at the boundary of the form

$$z^{j+1} = z^j + h\beta T^j z_s^j + h\gamma N^j z_\nu^j ,$$

where $z = x + iy$, the superscript j denotes the time step, z_s^j and z_ν^j are the numerically computed tangential and normal derivatives at time step j, T^j and N^j are the numerically calculated tangential and normal terms in square brackets in equations (3.7b) and (3.7c) which approach zero as $j \to \infty$, and β and γ are the tangential and normal convergence factors.

These factors, taken sufficiently small to produce a convergent scheme for a particular mesh size, are held fixed under mesh refinements so that the finite difference equations at the boundary remain the numerical analogs of the corresponding differential equations.

4.1.5. Convergence Rate of the Iterative Scheme

The convergence factors β and γ in the boundary equations and the dissipation parameter α in the interior equations must be chosen to produce a convergent scheme. The theory of the method of steepest descent indicates that these quantities have to be taken sufficiently small in order to avoid over-shooting the minimum point on the multi-dimensional surface described by the discrete formulations of the Dirichlet-Douglas functional 3.1 and the free boundary functional J_F of Section 3.3. Assuming that these parameters are appropriately chosen to produce convergence, linearized theory suggests that for sufficiently small mesh size the estimates

$$|x^{\infty}_{m,n} - x^{N}_{m,n}| \leq Ae^{-\lambda Nh}$$

$$|y^{\infty}_{m,n} - y^{N}_{m,n}| \leq Ae^{-\lambda Nh}$$

$$|\psi^{\infty}_{m,n} - \psi^{N}_{m,n}| \leq Ae^{-\lambda Nh}$$

are valid for the rate of convergence to the steady state finite difference solution, just as estimate (4) holds for equation (2). Here A and λ are constants independent of h and

λ is related to the lowest eigenvalue of the linearized problem. If α, β, and γ are held fixed under mesh refinement, then we expect the number of iterations N to grow like $1/h$. We should observe, in this connection, that this rate is the fastest that can be expected when the boundary is shifted using a forward difference for the time step. In particular, there is no advantage to using more sophisticated schemes (such as alternating-direction methods) on the interior equations, because the boundary shifts will still keep the overall convergence rate at $O(1/h)$. Furthermore, the computation time T increases like $1/h^3$, because the number of mesh points grows like $1/h^2$, and the total computing time is given approximately by

$$T = kMN \ ,$$

where k is the time to compute at a single mesh point, M is the total number of mesh points and N is the total number of iterations required for convergence.

4.2. Cusped Geometry Model

The numerical method was applied first to the cusped geometry problem described in Section 2.1 because it provides a relatively simple example on which to check the validity of the scheme. In this model no attempt is made to map corners of the rectangle into the separation points. Also, the ψ equation does not enter into the calculations. Thus we are dealing essentially with the problem of obtaining a suitable

periodic conformal mapping of the rectangle onto an annulus whose outer boundary is constrained in a special way.

4.2.1. Formulation of the Equations

Considerations of symmetry permit the problem to be formulated as a mapping from a rectangle R onto the physical domain D_z in the first quadrant of the z-plane as shown in Figure 4.3. The base AB of the rectangle is required to map onto the outer boundary $\Gamma + \Gamma_F$ of the annulus, where Γ is the free boundary and Γ_F is the fixed boundary consisting of portions of the walls $x = \ell$ and $y = \ell$. The parameter ℓ is arbitrary, and defines the basic periodic structure of the model. The points S_1 and S_2 denote the separation points between Γ and Γ_F. Their location on the walls is unknown and must be found as part of the solution. Our problem is to determine the conformal mapping of R onto D which has the boundary correspondence indicated in Figure 4.3, and for which Γ is located so that the free boundary condition holds along it. We do this by solving the numerical analog of the following system of time-dependent equations which result from the general theory:

(10a) $$x_t = \alpha \Delta x \ , \quad y_t = \alpha \Delta y$$

in R. In practice these equations are modified by the use of successive over-relaxation, as described in Section 4.1.2. On the boundary of R we obtain from the general theory

(10b) $$x_t + iy_t = -\beta[(x_u x_v + y_u y_v)/(x_u^2 + y_u^2)](x_u + iy_u)$$

along CD, where the convergence factor β is positive, and

(10c) $$x_t + iy_t = \beta[(x_u x_v + y_u y_v)/(x_u^2 + y_u^2)](x_u + iy_u)$$
$$+ \gamma[x_v^2 + y_v^2 - (x_u^2 + y_u^2)_o](x_v + iy_v)$$

along AB. On the segments AS_1 and S_1B which are supposed to map onto the walls Γ_F we effectively set γ equal to zero so that these points are subjected to a tangential shift only. The segment S_1S_2 maps onto the free boundary Γ and here both normal and tangential shifts are applied with positive convergence factors β and γ. We observe that the location of the images S_1 and S_2 must be found, that is, it is not known which points on AB map onto Γ and which map onto Γ_F. The correct apportionment is determined as the problem converges to a steady state. Provision must be made which allows points to move to either Γ or Γ_F as $t \to \infty$. We describe the technique for doing this in Section 4.2.3. The remaining boundary conditions are

(10d) $$x_u = 0 , \quad y = 0$$

on AD, and

(10e) $$x = 0 , \quad y_u = 0$$

on BC. These conditions are imposed by symmetry. They are

obvious consequences of the Schwarz reflection principle, but can also be derived from our tangential boundary conditions. For example, on AD, since we have

$$y \equiv 0 ,$$

we also have

$$y_v = 0 ,$$

so that the tangential equation (3.7b) reduces in this case to

$$x_t = \beta x_u$$

$$y_t = 0 \quad (y = 0) .$$

Since we expect $x_t \to 0$ in the steady state, we simply set x_u equal to zero at each iteration by an appropriate reflection in the finite difference equations for (10a).

The stream function does not appear in our formulation. As shown in Section 2.1, its solution to the Dirichlet problem in the rectangle is simply

$$\psi(u,v) = v/b .$$

The stream function enters into the conformal mapping problem only through the normal shift term along the free boundary. Since in this model we have

$$\psi_v = 1/b ,$$

the constant b can be absorbed into the convergence factor γ so that equation (10c) contains no trace of ψ.

4.2.2. Initial Mapping

The essential features required for the initial mapping are that it be univalent and that it possess the correct boundary correspondences to the extent possible. The requirement for univalence is necessary because there is no explicit mechanism in the numerical scheme to prevent overlapping of points, particularly those on the boundaries. The requirement for the appropriate initial boundary correspondences means that the initial mapping takes the line CD of the rectangle onto the arc CD of the physical plane, and takes the vertical sides onto the corresponding parts of the physical plane as indicated in Figure 4.3. The image of the base AB of the rectangle cannot be specified as completely. It is precisely its location which is to be found as $t \to \infty$.

In practice we chose the rectangle dimension $a = \pi/2$ and b equal to a rational multiple of a so that mesh spacing in horizontal and vertical directions can be taken equal. The inner radius r was chosen to be

$$r = e^{-b}$$

With this scaling the analytic function

$$z = e^{iw} \tag{11}$$

maps R onto the part of the annulus $r \leq |z| \leq 1$ which lies in the first quadrant, so that for $\ell \geq 1$, (11) is the trivial

solution to the problem. For non-trivial solutions we must choose ℓ in the range

$$r < \ell < 1 .$$

This requires the physical domain D_z to distort by pushing outward, establishing the boundaries Γ_F along the walls $x = \ell$, $y = \ell$, and yielding a conformal mapping with the same conformal type as the annulus.

A possible initial mapping which satisfies the requirements given above is

$$z = [(\ell-r^2)e^{-v}+r^2(1-\ell)e^{v}]/(1-r^2)e^{iu}$$

which takes R onto the part of the annulus $r \leq |z| \leq \ell$ which lies in the first quadrant. Its real and imaginary parts are harmonic and the steady state tangential condition

$$x_u x_v + y_u y_v = 0$$

is satisfied. For the normal shift, we have, initially,

$$(12) \qquad x_v^2 + y_v^2 - (x_u^2 + y_u^2)_o = -2r^2(1-\ell)(\ell-r^2)/(1-r^2)^2 < 0 ,$$

and since this quantity is negative, the outer circle $|z| = \ell$, which is the initial guess of Γ, will be pushed outward toward the walls $x = \ell$, $y = \ell$. The technique for dealing with the constraint that points must not move beyond these walls is described in the next section.

4.2.3. Boundary Conditions

When steady state is achieved in equations (10), the free boundary condition

$$x_v^2 + y_v^2 - (x_u^2 + y_u^2)_o = 0$$

is satisfied on Γ, and the mapping is conformal in consequence of the general theory described in Section 3.4. For the way in which we have formulated the cusped geometry model, provision must be made that the proper apportionment of points between the fixed boundary Γ_F and the free boundary Γ evolves as $t \to \infty$. To describe our method for achieving a stable configuration of the outer boundary $\Gamma + \Gamma_F$, we define S to be the domain bounded by the coordinate axes, the lines $x = \ell$, $y = \ell$ and the circle $|z| = r$. As we have observed in the previous section, if $\ell > 1$ then the solution we seek reduces to the trivial conformal mapping

$$z = e^{iw}$$

for the scaling we have chosen. If $\ell < 1$ then it is clear that the physical domain D_z must fill out an appropriate portion of S in order to be the image by a conformal mapping of R, which has the same conformal type as the above trivial solution. For this conformal mapping a certain number of points along AB will have their images on the walls $x = \ell$, $y = \ell$, forming the fixed boundary Γ_F, and the rest will map onto Γ, which will be located in the interior of S. We describe two

possible extreme configurations which demonstrate that the normal shift controls the convergence to the mapping with the correct conformal type. Consider the initial mapping given in the last section. Here Γ_F consists only of the endpoints ℓ and $i\ell$, where $\ell < 1$. As we see by inspection of equation (12), the normal shift term tends to push the initial free boundary outward. This motion results in points near the ends of the outer boundary becoming attached to walls so that they become part of Γ_F. On the other hand, consider a mapping which fills out a substantial portion of S so that Γ consists of a sharply rounded segment near the corner $\ell + i\ell$ of S, and suppose that all steady state equations in R and on its boundary are satisfied with the exception of the normal shift term. We use a local argument which suggests that the normal shift will push points inward, away from the corner. The derivatives with respect to u and v are high along the rounded segment; specifically, they are larger than the average $(x_u^2 + y_u^2)_o$ taken over Γ, so that the normal shift drives points inward, and in particular it will move points away from the walls so that they become part of Γ.

Between these two extreme mappings it is plausible that a stable configuration exists with the proper conformal type. We build into the formula (10c) by which the boundary points along AB are shifted a mechanism which senses the current state of the outer boundary and adjusts points according to rules which are suggested by the behavior of the extreme cases examined above. At time t, points along AB have their images

distributed along the current boundaries Γ and Γ_F. The average $(x_u^2 + y_u^2)_o$ is computed over those points which map onto Γ. Using this value, normal and tangential shifts are computed for the image of every point on AB. If the shifted image lies within S, then it is part of the free boundary Γ. In particular, a point previously on Γ_F can become part of Γ in this way, if the effect of the normal shift is to drive it away from the wall into S. If the shifted point lies outside of S, then the normal shift term is dropped, and the shift is modified so that the image is pasted to the wall at a location determined by the tangential shift alone. Such a point is part of the fixed boundary Γ_F. A point previously on Γ can become part of Γ_F in this way, if the normal shift term tends to drive it outside of S. We observe that this recipe provides a technique for attaching points to, or detaching points from, the walls $x = \ell$, $y = \ell$, in order to achieve the proper conformal type. The locations of the separation points S_1 and S_2 between Γ and Γ_F are determined as the solution approaches a steady state. We found this scheme to be highly stable. However, there are large truncation errors in the vicinity of the separation points S_1 and S_2 because no provision has been made to deal with the singular behavior there. Moreover, the discrete images which define the endpoints of Γ are really only approximations, presumably lower bounds, to the locations of the actual separation points of the continuous model.

The algorithm for treatment of these boundary points at time t is given below. At this stage of the computation we have available all derivatives necessary to apply equation (10c). We also have tags on each boundary point to determine which are on Γ and which are on Γ_F.

1] Compute the average $(x_u^2 + y_u^2)_o$ for those points currently tagged as members of Γ.

2] For each point z on AB:

a) Compute the point z' given by the finite difference analog of equation (10c),

$$z' = z + z_N + z_T,$$

where z_N and z_T are the total normal and tangential shifts.

b) Compare Re (z') and Im (z') with ℓ:

i) If Re (z') $< \ell$ and Im (z') $< \ell$

then tag z' as a point on Γ.

ii) If Re (z') $\geq \ell$

then modify z' by the formula

$$z' = \ell + i \text{ Im } (z + z_T)$$

and tag z' as a point on Γ_F.

iii) If Im (z') $\geq \ell$

then modify z' by the formula

$$z' = \mathrm{Re}\ (z + z_T) + i\ell$$

and tag z' as a point on Γ_F.

We remark that the above considerations are in sharp contrast to the situation which prevails if the value of the constraint ℓ is taken greater than 1 so that the solution is the trivial one. In this case the entire outer boundary of the annulus is the free boundary. In terms of the above algorithm, the cases 2b ii) and 2b iii) never occur. The separation points coincide with the corners A and B, and the model is quite similar to the rectangle mapping discussed in Section 3.5.

The boundary CD of the rectangle maps onto the circle Ω of radius r in the physical plane. The tangential shift (10b) is applied to each point z on this boundary and yields a new point z_1 which is not necessarily on Ω because of the finite difference approximations. A second order normal shift of the form

$$z' = r\ z_1/|z_1|$$

is applied to obtain the new point z' on Ω.

4.3. Hydrodynamics Models

The application of the numerical method to the solution of the hydrodynamics models includes an important additional feature, not present in the cusped geometry model. For these examples, the conformal mapping is set up so that the separation

point z_o in the physical plane is the image of one of the corners w_o of the rectangle. This means that the conformal mapping has the expansion

$$z = z_o + a(w - w_o)^2 + \ldots$$

about the corner. Since the theory shows that the stream function is regular in powers of $(z-z_o)^{1/2}$ near the separation point, we obtain the expansion for $\psi(w)$ at the corner in the form

$$\psi = a_o + \mathrm{Im}\,[a_1(w-w_o) + a_2(w-w_o)^2 + \ldots]$$

in the plane case. (The coefficient a_1 is actually zero since the speed at z_o is finite.) A similar result holds in the axially symmetric case. The effect of this feature of the conformal mapping is to make z and ψ regular functions of w about w_o, so that the over-all finite difference method is accurate to second order in mesh width h. Thus we expect to be able to approximate the continuous solution as closely as we like by taking a sufficiently fine mesh. On the other hand, the introduction of this procedure makes the problem of producing a numerically convergent scheme considerably more delicate by comparison to the cusped geometry model which, though crude, is highly stable. We indicate the difficulties and our methods for dealing with them in the subsequent sections.

We also solve axially symmetric hydrodynamics models to show that our method can be applied more generally. We find

that there are no significant additional considerations involved in making the scheme convergent for this case, beyond obvious programming changes. In the following sections we give the details of the formulation for the vena contracta model. The application to the Riabouchinsky model is essentially the same.

4.3.1. Formulation of the Equations

We set up the problem for the truncated model described in Section 2.3. We seek the conformal mapping from the rectangle R onto the physical domain D_z with the boundary correspondences shown in Figure 4.4.

In accordance with our numerical procedure, we solve the numerical analogs of the following equations:

$$x_t = \alpha \Delta x$$

$$y_t = \alpha \Delta y \tag{13a}$$

$$\psi_t = \alpha(\Delta\psi - (m/y)\nabla y \cdot \nabla\psi$$

in R. In practice, these equations are modified by the application of over-relaxation, as described in Section 4.1.2. On the boundary CM we have

$$x = \ell$$

$$y_u = 0 \tag{13b}$$

$$\psi_u = 0$$

and on BC we have

$$x_v = 0$$

(13c) $$y = 0$$

$$\psi = 0$$

These conditions result from considerations of symmetry. Because of the way we treat the point at infinity, the first of equations (13b) is actually different from the one shown. We will describe the change in detail in Section 4.2.4. On MA + AB the boundary condition for the stream function is

$$\psi = 1 \ ,$$

in accordance with the normalization introduced in Section 2.3. For the conformal map, the tangential condition reduces to

$$x = 0$$

(13d)

$$y_t = -\beta y_u$$

along AB, using the fact that x_v is identically zero. On the boundary MA, which is supposed to map onto the free boundary Γ in the physical plane, we have

$$(13e) \quad x_t + iy_t = \beta\left[(x_u x_v + y_u y_v)/(x_u^2 + y_u^2)\right](x_u + iy_u)$$

$$+ \gamma\left[\frac{y^{2m}(x_v^2 + y_v^2)/\psi_v^2}{1/\lambda^2} - 1\right](x_v + iy_v) \ .$$

The appropriate choice for λ is described in Section 4.3.5. In

the formulation given by equations (13), we observe that the ends of the free boundary A and M in the physical plane are permitted to slip in the vertical direction. The point M is actually shifted in response to the normal term in (13e) only, since the tangential shift is always zero at M, by symmetry. The separation point A receives a tangential shift according to a special formula. The adjustment of the separation point is quite critical because its location determines the conformal type of the mapping, which is a global characteristic. We discuss this aspect of the problem in Section 4.3.5.

4.3.2. Initial Mapping

As with the cusped geometry model the important requirements for the initial mapping are that it be univalent so that there is no initial overlapping, and that it produce the proper boundary correspondence to the extent possible. In practice, the initial data was set up in either of two ways.

1) We utilized the solution to the plane infinite jet model given by equation (2.9) coupled with the analytic function

$$(14) \qquad \zeta(w) = 1/\pi \log\left[-(1+\cos h(w-a)\pi/b)/2\right] ,$$

which maps the rectangle

$$R: \quad 0 \leq \mathrm{Re}\,(w) \leq a$$

$$0 \leq \mathrm{Im}\,(w) \leq b ,$$

onto the semi-infinite strip

$$D_\zeta: \qquad -\infty \leq \mathrm{Re}\ (\zeta) \leq \zeta(0,v)$$

$$0 \leq \mathrm{Im}\ (\zeta) \leq 1 \ .$$

Examination of the boundary correspondence shows that the composite function given by (2.9) and (14),

$$z = z(\zeta(w)) \ ,$$

maps R onto a portion of the flow region of the infinite jet which excludes only the tail of the jet as $x \to \infty$. The effect of omitting this piece is to truncate the infinite jet downstream from the orifice at a location $x = \ell$ which goes to infinity linearly with a. The composite function and equation (14) provide initial data for ψ and z in terms of w which satisfy all steady state equations for the plane model except where the jet is truncated. We set the initial value of the jet length ℓ by putting

$$x(0,v) = \mathrm{Re}\ (z(0,v)) = \ell \ .$$

2) The second method of setting up initial data was used when the mesh was refined by a factor of two. Given the numerical solution for a mesh h, we interpolated values at the new mesh points to obtain initial data. This method was especially useful for the axially symmetric model where the truncated plane jet was actually poor initial data for refined meshes.

4.3.3. Conditions at Infinity

The conformal mapping we seek takes the corner B of the rectangle into infinity of the z-plane, as indicated in Figure 4.4. Analysis of the boundary correspondences shows that $z(w)$ has a simple pole at the point $w_B = a + ib$. Also, the stream function ψ is discontinuous at w_B, with the value zero along BC and unity along AB. We deal with this behavior by introducing an interface in R, shown by the dotted lines in Figure 4.4, which defines a triangular subdomain R_1. In R_1 the equations are modified by subtracting off the singular behavior of z and ψ. Specifically we define the functions

(15a) $$z_R(w) = z(w) - p/(w-w_B)$$

where p is the pole strength, and

(15b) $$\psi_R(w) = \psi(w) - \psi_m$$

where

$$\psi_o = 2(1 - \theta/\pi)$$

and

$$\psi_1 = 1 + \cos\theta$$

As usual, m = 0 corresponds to plane flow and m = 1 corresponds to axially symmetric flow, and θ is the angle in the polar representation of a point in D_z. The functions ψ_m describe the asymptotic behavior of ψ as $|z| \to \infty$ in the second quadrant.

In R_1 we solve numerically for ψ_R and z_R. The equations for z_R and ψ_R are the same as for z and ψ, because the functions

subtracted off are themselves solutions to the corresponding interior differential equations. The boundary conditions for z_R and ψ_R take the form

$$x_R = 0$$

$$(y_R)_t = -\alpha(y_R)_u$$

$$\psi_R = 0$$

on the vertical boundary of R_1, and

$$(x_R)_u = 0$$

$$y_R = 0$$

$$\psi_R = 0$$

on the horizontal boundary of R_1. The boundary conditions on the interface are determined by an overlapping of the boundary between R and R_1. This interface consists of two fixed parallel lines ℓ_1 and ℓ_2 which run diagonally through the mesh as shown in Figure 4.5. An iteration of equations (13a) at a given time step is carried out in the following sequence:

1) The values of z and ψ on ℓ_2 are used as boundary conditions in an iteration of the mesh points of $R-R_1$.

2) Transformations (15) are applied to z and ψ along ℓ_1 and ℓ_2 to compute z_R and ψ_R.

3) The values of z_R and ψ_R along ℓ_1 serve as the boundary conditions in an iterative sweep through the mesh points of R_1.

4) Transformations (15) are applied along ℓ_1 and ℓ_2 to replace z_R and ψ_R by z and ψ again.

The process is repeated at each iterative cycle. The values of z and ψ are altered along ℓ_1 by step 1 and along ℓ_2 by step 3. As $t \rightarrow \infty$ we approach a steady state.

In the axially symmetric case the additional transformation

$$\psi_R^* = |Z|\psi_R$$

described in Section 4.1.3 is used in R_1 in order to keep the truncation error $O(h^2)$. Thus we actually solve numerically for ψ_R^* in R_1.

The pole strength p is an arbitrary parameter of the problem when infinity is treated in this way. In practice we chose its value to be $8b/\pi(\pi+2)$, which is the pole strength in the analytic solution for the plane infinite jet. This value is used for both plane and axially symmetric models.

4.3.4. Shift of the Line of Symmetry ℓ

The strength of the pole becomes an input parameter as a result of our method of dealing with infinity. Therefore the problem as formulated by equations (13) is over-determined. We compensate by permitting the entire line of symmetry $x = \ell$ to shift horizontally, which allows the jet length to be variable. This shift is imposed according to the formula

(13f) $$\ell_t = \delta(x_v^2 + y_v^2 - x_u^2 - y_u^2)_o \ ,$$

where δ is a positive convergence factor and the subscript on the right indicates an appropriate average over R. Equation (13f), which we call the ℓ-shift, replaces the first of equations (13b) as the boundary condition on the vertical side CM of the rectangle. Our reason for expecting a recipe such as (13f) to converge is similar to the analysis given in Section 3.5 for rectangular domains. Suppose it is possible to achieve a steady state solution of the interior equations and the tangential boundary conditions. The theory asserts that the quantity $x_v^2 + y_v^2 - x_u^2 - y_u^2$, which we denote by H, is identically constant. Suppose that the value of ℓ in this solution is too large. Then we may assume that there exists a rectangle R', whose length-to-width ratio is larger than that of R, which our solution maps conformally onto the flow region. The mapping from R to R' is an affine transformation which stretches points in the u-direction. Therefore we observe geometrically that points in the tail of the jet are stretched in the x-direction which means that the u-derivatives there are larger than the v-derivatives. It follows that H is negative and so ℓ_t is negative in accordance with (13f). The same reasoning applies if the jet length is too small, in which case ℓ_t is positive. A steady state is reached when H is zero.

4.3.5. Separation Point

The separation point z_o is shifted according to appropriately applied tangential formulas, with the constraint that it lies on the line $x = 0$. As with the cusped geometry model, the determination of the proper conformal type of the physical domain is an important part of the problem. For a rectangle in the w-plane with a given length-to-width ratio, we expect to achieve a conformal map onto the physical domain which satisfies the free boundary condition only if the separation point is properly located on the y-axis relative to the jet length. In the cusped geometry model, the conformal type is established by the normal shift term only, with certain constraint conditions along the walls $x = \ell$, $y = \ell$ as discussed in Section 4.2.3. In that formulation, the apportionment of points between fixed and free boundaries is not specified, but is determined as the scheme converges. The situation is essentially different in this respect for the vena contracta model. We require a specific point on the rectangle, namely the corner w_o, to map into the separation point z_o, so that the number of points which map onto the free and fixed boundaries is specified. Since z_o is shifted sensibly only according to tangential terms on the boundary, we see that the normal and the tangential shift must work together to yield the proper conformal type. This is one of the aspects of the formulation of the vena contracta model which makes the issue of convergence considerably more delicate than it is for the cusped geometry model.

The formulas which we use to shift the separation point are based on the geometrical interpretation of the tangential shift condition. In general, a steady state is reached when inner normals on R map into inner normals on D_z. At the separation point, where the right angle at the corner w_o is supposed to map onto a 180^o angle at z_o, a conformal map will carry a line s which bisects the right angle in R onto a line s' normal to the 180^o angle in D_z. Since the 180^o angle is oriented in the vertical direction, this normal s' is a horizontal line, as shown in Figure 4.6. Therefore, a reasonable way of setting up the tangential shift at the separation point is to use the formulas

$$x = 0$$

(13g)

$$y_t = \alpha[(-y_u + y_v)/\sqrt{2}] \ .$$

The term in square brackets is the derivative of y in the s-direction and steady state is achieved in this formulation when the line s' becomes horizontal, characterizing the angle-doubling property of the conformal map. Another way of looking at these formulas is to observe that the separation point can be shifted according to the tangential conditions from either the fixed boundary, where the fact that x_v is identically zero yields the formulas

$$x = 0$$

$$y_t = -\alpha y_u \ ,$$

or from the free boundary, where, if we assume that x_u is zero which it is supposed to be in the steady state, the formulas are

$$x = 0$$

$$y_t = \alpha y_v \ .$$

Apart from the factor $\sqrt{2}$, formulas (13g) represent an average of these tangential conditions.

We argue that any reasonable method, such as given by (13g), for treating the separation point which results in an over-all convergent scheme will yield a finite difference solution which approximates the continuous solution. This is because the solution to the continuous problem is known to be unique, and in particular, there is only one conformal mapping from the rectangle onto the physical domain which satisfies the free boundary condition.

We obtain an additional benefit from the point of view of stability by use of (13g). The finite difference analog of the expression $-y_u + y_v$ can use simple forward differences to approximate the derivatives instead of the usual three-point formulas and we still retain second order accuracy in mesh size h. Specifically, the relation

$$-y_u + y_v = (y_2 - 2y_o + y_1)/h + O(h^2)$$

holds in the steady state at the corner w_o, where the points are labelled as shown in Figure 4.6. This follows from application of a Taylor series expansion about the corner and use of the fact that the solution for y satisfies Laplace's equation at the corner in the steady state, which eliminates the first power of h in the expansion. The use of three points, instead of five, to describe the motion of the separation point as $t \to \infty$, tends to improve the stability of the computation.

4.3.6. Free Boundary Condition

The speed q at any point along the free boundary Γ is given by

$$q^2 = y^{-2m}\psi_v^2/(x_v^2 + y_v^2) \ .$$

The significance of λ in the normal shift term of equation (13e) is that its value at any time t is an estimate of the constant speed q_o along Γ, and so in what follows we write $1/q_o^2$ instead of λ^2. We seek the steady state condition

$$q_o^2/q^2 - 1 = 0$$

by adjustment of the free boundary normal to itself according to equation (13e).

The choice for $1/q_o^2$ of the average

$$1/q_o^2 = [y^{2m}(x_u^2 + y_u^2)/\psi_v^2]_o$$

over the free boundary, which is successful in the cusped geometry model, yields an unstable scheme for this case, as shown by the following heuristic reasoning. Suppose the free boundary develops a corner at the separation point as the time-dependent problem is being solved. Then, under the assumption that the discrete solution at this stage of the computation approximates some sort of flow, the speed q at the separation point is high relative to its average value q_o over the free boundary, and we have

$$q_o^2/q^2 - 1 < 0$$

near the separation point. Since the normal (x_v, y_v) is directed into the physical domain, the free boundary near the separation point is shifted outward, tending to increase the sharpness of the corner. The same argument shows that a bulge in the free boundary at the separation point will also be accentuated, hence instability of the free boundary at the separation point results from the averaging formula.

The choice suggested by the above analysis of instability is to make $1/q_o^2$ correspond to the speed at the separation point itself. Thus, for example, if a sharp corner develops, the separation point speed q_o is <u>larger</u> than the speed at nearby free boundary points, so that the normal shift sends these points <u>into</u> the flow region, correcting the sharp corner. The estimate of q_o must be obtained as a limit of the speed along the free boundary Γ as we approach the separation point and this computation is carried out numerically by fitting a linear function to

values of $1/q^2$ nearby and extrapolating to the separation point. The slope of this linear function must go to zero as $t \to \infty$. When the slope is different from zero, it essentially provides a stabilizing correction to the averaging formula.

We must retain in the normal shift formula the provision for making the conjugate function $x_v^2 + y_v^2 - x_u^2 - y_u^2$ equal to zero in the steady state. The general theory shows that this function is equal to a constant H when the Dirichlet-Douglas functional is minimized, so that if H = 0 at even one point on the boundary, for example the separation point, then it is zero throughout R. To achieve the condition H = 0, we must incorporate u-derivatives, which are tangential derivatives on Γ, into the normal shift formula. We recall that in the cusped geometry model this is achieved by use of an average of $x_u^2 + y_u^2$ over Γ so that as $t \to \infty$ the condition H = 0 is obtained numerically, not just at one point, but over the whole free boundary. Although the theory suggests that we could use the value of $x_u^2 + y_u^2$ at just one point on the free boundary in the normal shift formula, such a formulation is not expected to produce a stable scheme. The situation is analogous to solving an elliptic equation in which we specify a directional derivative with a non-zero tangential component, that is, a u-derivative along the boundary, and such problems are difficult to treat. The use of averaging, equivalent to integration along the boundary, is one way out of the difficulty. For the vena contracta model, we have shown that this does not work. We are forced to use a value of $1/q_o^2$

based on a single point, and u-derivatives in the extrapolation cause instability. Therefore we must use v-derivatives, which are normal derivatives on the free boundary, to estimate $1/q_o^2$ at the separation point, and we are still faced with the task of building into the normal shift formula a mechanism which yields H = 0 in the steady state. We do this by numerically imposing the requirement that the speed be continuous at the separation point. Continuity of the speed is implicit in the continuous formulation of the problem, but not in the discrete formulation, where it must ultimately be allied with the conformality of the mapping.

Our requirements lead us to the specification for $1/q_o^2$ as the weighted average given by

$$1/q_o^2 = (1-\varepsilon)/q_1^2 + \varepsilon/q_2^2 \tag{16}$$

where ε is the weight parameter, chosen experimentally to produce convergence, and q_1 and q_2 are the speeds extrapolated from the free boundary and the fixed boundary, respectively, given by the limits

$$1/q_1^2 = \lim_{\substack{u\uparrow a \\ v=0}} [y^{2m}(x_v^2 + y_v^2)/\psi_v^2]$$

$$1/q_2^2 = \lim_{\substack{u=a \\ v\downarrow 0}} [y^{2m}(x_u^2 + y_u^2)/\psi_u^2] \ .$$

These limits are evaluated numerically by extrapolation of a

linear function which fits the data in a least squares sense at a suitable number of points. On the free boundary, the truncation error is not affected by the number n_e of points used. In steady state the slope of the linear function is zero because the speed is constant all along the free boundary. The number n_e is therefore chosen solely on the basis of stability. On the fixed boundary, the speed is not constant so that the number n_e' of points used in the linear extrapolation should be taken as small as possible consistent with stability. Of course we need a minimum of 2 points in order to define a slope.

The conditions that the speed is continuous and that H is zero in steady state are achieved in the following way. From the steady state normal shift term in (13e) we have

$$q_o^2/q^2 = 1$$

along Γ, so that the free boundary condition is satisfied. As a consequence, we must also have

$$1/q_1^2 = 1/q_o^2$$

since $1/q_1^2$ is an extrapolation of the (constant) values of $1/q^2$ along the free boundary. Therefore, by inspection of equation (16) we also have

$$1/q_2^2 = 1/q_o^2 \ ,$$

so that the speeds q_1, q_2 and q_o are all equal. To show that H is zero we argue that since ψ_u and ψ_v both go to zero, and the limits $1/q_1^2$ and $1/q_2^2$ are finite at the separation point, then it must follow that the quantities $x_v^2 + y_v^2$ and $x_u^2 + y_u^2$, which are the numerators in these limits, also both go to zero there. In this way we obtain

$$H = 0$$

at the separation point, and by the general theory, the mapping is conformal. We remark that there is an analytic reason why the weight factor ε should have to be chosen small. If there exist solutions to the differential equations which satisfy all steady state conditions with the exception that the speed is not necessarily continuous at the separation point, then these solutions have the property that both x_v and y_v are zero at the separation point because the limit of speed coming from the free boundary is finite. Also, by the way we treat the tangential shift of separation point, the derivative y_u is zero. There is no control, though, on x_u, which can be different from zero. The result is that $1/q_2^2$, the limit from the fixed boundary side of the separation point, is infinite, due to the non-zero x_u. A small ε is necessary to prevent instability caused by the development of large values of $1/q_2^2$ as the scheme converges.

4.3.7. Riabouchinsky Model

The application of the numerical method to the Riabouchinsky model is the same as it is for the vena contracta, and so we shall omit the details. Here also, by mapping a corner of the rectangle into the separation point, we uniformize the singularity in the stream function, and make the over-all scheme accurate to second order in mesh width h. The following observations are noted:

1) The tangential shift of the separation point, calculation of the speed as a weighted average of the limits from the free and fixed boundaries, the introduction of an interface near infinity and subtraction of the pole in the desired conformal mapping, and the associated horizontal shift in the vertical line of symmetry of the flow, which are techniques we have described in detail for the vena contracta model, are carried over and applied in exactly the same way for the Riabouchinsky model.

2) The stream function can be written in the form

$$\psi = Uy^{1+m}/(1+m) + \psi_R$$

where the regular part $\psi_R \to 0$ as $|z| \to \infty$. In the triangular subdomain R_1 defined by the diagonal interface we solve numerically for ψ_R in the plane case (m = 0), and for ψ_R^* in the axially symmetric case (m = 1), where

$$\psi_R^* = |Z|\psi_R \ .$$

Here the Kelvin inversion (Section 4.1.3) takes the slightly different form

$$Z = \frac{1}{z-\ell}$$

to account for the ℓ-shift.

3) The boundary correspondences for the conformal map are in accordance with those given in Figure 2.3a and 2.3c, for both the plane and axially symmetric models. The initial mapping is taken in either of two ways. In the plane model it is the exact solution to the plane flow model given by equation (2.6), for a specific value of k. It is possible to choose k so that the dimensions of the rectangle K and K' have a rational ratio, allowing for equal mesh spacing. In the axially symmetric model, the plane solution is used as the initial mapping for crude mesh widths, and for finer meshes an interpolated solution is used.

4.3.8. Remarks

We view the following features as the three delicate aspects of the numerical method:

1) The equations (13g) for shifting the separation point.

2) The specification of $1/q_o^2$ by equation (16) in the normal shift term.

3) The treatment of the neighborhood of infinity and the associated ℓ-shift (13f) of the vertical line of symmetry.

The formulas and procedures used were arrived at for the most part experimentally. Taken individually, there are many

reasonable ways in which to deal with each of these aspects. However, in practice we found that it was a more difficult task to make them all work together. It is not yet entirely clear why some ideas failed and the ones we have given were successful. Moreover, it is quite probable that still other approaches can greatly improve the convergence properties compared to what we have achieved to date.

We include a final remark on the heuristic explanations of several aspects of the scheme. We use formulas which make the quantity

$$H = x_v^2 + y_v^2 - x_u^2 - y_u^2$$

equal to zero both at the separation point and in the ℓ-shift formula. This is really contradictory, since the theory says that when we have

$$x_u x_v + y_u y_v = 0$$

on ∂R, then the harmonic conjugate H is identically constant throughout R. A more sophisticated theory takes into account the fact that the analytic function $z(w)$ has a pole at one of the corners of R, the treatment of which necessitated the addition of the ℓ-shift (13f) in the first place. The harmonic function $x_u x_v + y_u y_v$ also has a pole at this corner, which means that it is possible that it can be zero everywhere else on the boundary of R, without being zero in the interior. In consequence, the normal derivative of the harmonic conjugate H is

zero on ∂R, but H is not necessarily constant in R. This is analogous to the example of the function $f(z) = z$, whose imaginary part y is zero on the x-axis, and positive in the upper half-plane, and whose real part has a vanishing normal derivative on the x-axis, and a nodal line ($x = 0$) extending to infinity. In our numerical scheme, we impose the condition $H = 0$ at the separation point as described in Section 4.3.6. This means that we obtain a nodal line ($H = 0$) which emanates from the separation point and runs into R. We reason that this nodal line must not be allowed to wander off to the corner at which the pole is located, for by analogy with the above example of $f(z) = z$, such behavior means a non-unique solution (cf. the Phragman-Lindelof principle). We therefore use the ℓ-shift formula to control the path of the nodal line so that it terminates on some other part of ∂R, thereby enclosing some finite subdomain of R. If this is the case, then we can use well-known theorems to conclude that $H \equiv 0$ in this subdomain. From this it follows, by analytic continuation, that the analytic function for which H and $x_u x_v + y_u y_v$ are the real and imaginary parts, is identically zero throughout R, and we obtain the Cauchy-Riemann equations for $z(w)$.

5. RESULTS

The main result is that the numerical method, when applied to the models we have studied, is convergent for appropriately chosen factors. Results for the cusped geometry model indicate the expected high degree of stability except in geometric configurations for which the effects of truncation error at the separation point become pronounced. For the hydrodynamic models, both plane and axially symmetric calculations are performed for mesh widths sufficiently small to demonstrate that the numerical solution converges to the continuous solution. Computations show that the contraction coefficient and drag coefficient for the plane models agree to at least four significant figures with the exact values, and new estimates are obtained for these quantities in the axially symmetric case. Calculations are also described in which the method is applied as a technique for conformal mapping only.

5.1. Cusped Geometry Model

The geometric configuration for this model is controlled by specification of the wall constraint ℓ and the radius r of the coil. In practice, r was fixed by the height b of the rectangle according to the relation

$$r = e^{-b} ,$$

which scales the physical domain so that ℓ must be selected in the range $r < \ell < 1$ for non-trivial solutions.

The values of the convergence factors α, β, and γ were determined experimentally to produce rapid convergence consistent with the stability of the computation. The value of α must be sufficiently large to provide damping of the interior equations. Selection of α is equivalent to setting the value of the relaxation factor in these equations. The factors β and γ control the size of the motion of the boundary points. In accordance with the theory of the method of steepest descent, β and γ must be sufficiently small to prevent overshooting the minimum point of the multi-dimensional surface given by the numerical formulation.

Table I and Figure 5.1 summarize the results of a specific calculation. Our purpose in conducting this sequence of experiments is to examine the convergence properties of the iterative solution to a steady state answer, where steady state is defined as the reduction of all residuals to less than 10^{-8}. We also want to observe the behavior of the discrete solution as the mesh is successively refined. We note the following remarks.

1. The number of iterations required to reach steady state approximately doubles with each refinement of the mesh by a factor of two. This confirms the linear theory described in Section 4.2.3 which asserts that the number of iterations grows like $O(1/h)$.

2. About 19 micro-seconds are required to perform an iteration in both x and y at a single interior mesh point on

the CDC 6600 computer. At this speed the problem for the crude mesh h required about 9 seconds to converge, and the problem for the most refined mesh h/8 required about 56 minutes.

3. Figure 5.1 shows the computed free boundary for this geometric configuration using the data for the h/4 mesh. In this solution the walls Γ_F consist of 19 points each and the free boundary Γ is described by 75 points. The tabulation of the separation points S_1 and S_2 and the midpoint M in Table I for the various mesh widths indicates the expected behavior due to truncation error. The midpoint location is stabilized to three digits at (.719,.719) but the location of the separation points is known only to be in the range .21-.22. This is because no provision was made to deal with the known singular behavior at these points.

4. The cusped geometry model provides an example with a curved fixed boundary, namely the circular coil Ω, in which second order normal corrections are made to keep tangentially shifted points on the boundary, as described in Section 4.2.3. The procedure was quite satisfactory in this model and we expect that curved boundaries in general can be treated in the same way.

5. The initial mapping used for most runs was the transformation described in Section 4.2.2. In order to verify that the convergence is not one-sided, runs were also made in which the initial mapping specified a free boundary Γ close to the corner $\ell+i\ell$ so that the motion toward steady state was inward,

away from the corner. We were able to obtain convergence for a wide variety of such initial conditions, demonstrating the high degree of stability possessed by the scheme.

Experiments were also made in which the value of the wall constraint ℓ was reduced, requiring the free boundary Γ to move closer to the cover $\ell + i\ell$ in order to satisfy the condition of conformality. This effect reduces the number of points on the base of the rectangle which map onto Γ. The results of these calculations are qualitatively similar to what we have described in Table I. As Γ is reduced, however, the truncation error in the vicinity of the separation builds up rapidly due to the increased stretching of the physical domain. There is a fairly sharp threshold in ℓ, below which the free boundary appears to "roll up" toward the corner and is numerically described by just one point, the midpoint M, with all the other points pasted to the walls Γ_F. Refinement of the mesh is necessary to retain accuracy of the numerical solution. The same effect is observed when calculations are made with smaller values of the radius r. This behavior exemplifies the importance of treating the region near the separation point properly if a high degree of accuracy is to be attained.

Calculations were also made in which the wall constraint was removed, that is, $\ell > 1$. In this limiting case the separation points coincide with the corners of the outer boundary and are not singular points. In effect, this model is a variant of the trivial rectangle mapping described in Section 3.5.

Experiments verify that the convergence of the numerical solution to the continuous trivial solution $z = e^{-iw}$ is $O(h^2)$.

5.2. Hydrodynamic Models

In this section we describe the results of the calculations of the vena contracta and Riabouchinsky flows. These are models of the type for which the method was designed to be accurate to $O(h^2)$ by mapping a corner of R into the separation point. Our general results are as follows:

1. The scheme is convergent for a wide variety of geometrical configurations provided that the length to width ratio r of the parameter rectangle R is not too large. By taking the mesh width h sufficiently small we verified the convergence to be $O(h^2)$.

2. The method works equally well for axially symmetric and plane geometries.

3. Drag and contraction coefficients for the plane model agree with their exact values to almost four and almost five significant figures, respectively. For the axially symmetric models, new estimates of these quantities are obtained which are judged to be as accurate as the results of the calculations for the plane models.

The details are given in the following sections.

5.2.1. General Results

Calculations of the hydrodynamics models were made for various mesh sizes h and length-to-height ratios r of the parameter rectangle. In Figure 5.2 we give the results of

particular calculations in terms of graphs of the profiles of the free boundary for the plane and axially symmetric jet. In Figure 5.3, the same kinds of results are shown for the Riabouchinsky model. We observe the extremely fine resolution near the separation point, as shown in the enlarged inserts, where the actual data points are plotted. The high density of mesh points in this region is the consequence, numerically, of having mapped a corner of R into the separation point. For both models, the exact plane solution overlays the numerically computed solution for the resolution shown.

In practice, the various convergence factors which occur in the formulation of these problems were determined by trial and error to produce convergent schemes. These factors are listed below:

1) α - dissipation factor for the interior equations, which controls the damping (relaxation factor) in equation (4.1).
2) β, γ - convergence factors for the tangential and normal shifts at the boundary.
3) δ, R_δ - convergence factor for the ℓ-shift of the line of symmetry and the subdomain R_δ over which the average in (4.13f) is computed.
4) n_e, n_e' - number of points used in the extrapolation of the speeds from the free and fixed boundaries, respectively.
5) ℓ_c - the number of points along the vertical side of the rectangle above which the triangular subdomain R_1 is defined. This parameter locates the intersection of the diagonal interface with the vertical side of the rectangle.

6) ε - weight factor in the computation of the weighted average of speeds at the separation point.

In Table II we list the appropriate data for the specific cases we have given. Calculations were also made for various other values of r and h in order to obtain data for the contraction coefficients and drag coefficients. The following observations are pertinent for these runs:

1) Verification that the numerical solution converges with h to the continuous solution is given in Table III. Data is shown for a particular axially symmetric vena contracta and plane Riabouchinsky model. The quantities tabulated are the location of the line of symmetry ℓ and its u-derivative, which are typical data points. Calculations show that the convergence is $O(h^2)$ for sufficiently small h.

2) The success of the scheme was fairly sensitive to the choice of an initial mapping. In practice, for a calculation with a refined mesh, we found it best with the axially symmetric models to use as an initial mapping the solution previously calculated for a cruder mesh interpolated at the new mesh points. In some cases it was found expedient to heavily damp the time-dependent equations during the first few hundred cycles of iteration in order to smooth out the data. The number of iterations required for convergence obeys the linear theory of Section 4.1.5 for the axially symmetric vena contracta as shown by the data of Table III. On the other hand, Table III indicates a faster rate of convergence for the plane Riabouchinsky model.

This is because as the mesh is refined, the initial mapping provides better initial data so that the numerical solution starts closer to the final answer.

3) Experiments show that to iterate 1000 mesh points for 1000 cycles takes about 80 seconds for the axially symmetric case and about 35 seconds for the plane case on the CDC 6600 computer. In practice, some economy was achieved due to the fact that the convergence of the ψ equation was quite rapid. This permitted iteration of the ψ equation only once for every several cycles of iteration of the x and y equations. For the vena contracta model we were able to use a ratio of 1 to 10 in this scheme. For the Riabouchinsky model, where the ℓ-shift affects the ψ equation more directly, ratios of 1 to 5 were possible for the lower values of r, but we had to use a 1 to 1 ratio for the largest value r = 25/12. The actual computing time to reduce residuals below 10^{-6} was about 40 minutes for the plane vena contracta model and about 65 minutes for the axially symmetric vena contracta model of Table II.

4) Values of the weight factor ε in the range .02-.04 for the Riabouchinsky model and about .1 for the vena contracta model were found by experiment to produce convergent schemes. This confirms the analysis given in Section 4.3.6 that small values of ε are required in the formula for $1/q_o^2$.

5) The location of the interface, governed by the parameter ℓ_c, was determined experimentally, but also with the motivation that the derivatives along it should be reasonably close to

unity, so that the transmission of truncation error between the regions is minimized. In practice, we found that a variety of interface locations were acceptable to produce convergence.

6) Values of α, β, γ, and δ were found experimentally.

7) For the vena contracta model, the region R_δ, over which the average in equation (4.13f) is computed, was taken to be the entire rectangle excluding the triangular region R_1. In the Riabouchinsky model, experiments with large r have shown that a different choice of R_δ is necessary to produce convergence. We choose R_δ to be a fixed segment MA' along the base MA of the rectangle (Figure 2.3c). Furthermore, we normalize (4.13f) by dividing each term in the average by $x_u^2 + y_u^2 + x_v^2 + y_v^2$ so that all terms have equal weight. In view of the nodal line theory developed in Section 4.3.8, we argue that this recipe exerts a stronger influence in making the nodal line exit from the interior of R at a point along the base MA, whereas a choice of R_δ as in the vena contracta model permits the nodal line to wander off to the corner where the pole is located. Further experiments are in progress.

5.2.2. Contraction Coefficient

We used our numerical method to calculate the contraction coefficient C_m for the infinite jet ($r \to \infty$). The known value in the plane case ($m = 0$), is given by

$$C_o = \frac{\pi}{\pi+2} \doteq .611015 \ ,$$

and can be used to check the computation. In the axially symmetric case (m = 1), values of C_1 in the range .57 - .61 have resulted from various other techniques of estimation [5,6,13,14].

By using as long a rectangle and as small a mesh width as possible we find that the computed value of C_o is

$$C_o = .61129$$

which shows agreement with the exact answer to three digits. However, we can improve our estimate by making use of the expected asymptotic behavior of C_m as $h \to 0$ and $r \to \infty$ and performing suitable extrapolation of the data. In Section 2.3 we obtained a formula for this behavior, given by

$$C_m(r) \sim C_m + A_m e^{-\lambda_m r} \tag{1}$$

as $r \to \infty$, where the constant λ_m has the values

$$\lambda_o = \frac{\pi}{2} \doteq 1.6$$

$$\lambda_1 \cong 2.4 \quad .$$

We denote by $C_m(r,h)$ the numerically computed contraction coefficient for a given r and h. Since the numerical scheme is $O(h^2)$ this quantity should converge for fixed r with an error term $M_m h^2$. The number M_m differs from a constant by terms which go to zero exponentially with r. Likewise, for

fixed h, $C_m(r,h)$ converges with an error term $A_m e^{-\lambda_m r}$, where A_m and λ_m differ from constants by terms which are $O(h^2)$. Therefore, we expect the asymptotic behavior of $C_m(r,h)$ to be given by

$$C_m(r,h) \sim C_m + M_m h^2 + A_m e^{-\lambda_m r} \tag{2}$$

as $r \to \infty$, $h \to 0$, where A_m, λ_m and M_m are assumed constant. To carry out our estimate we made a series of computations of $C_m(r,h)$ which are summarized in Table IV and Table V. The columns of these tables indicate the ratio r. The rows indicate mesh refinements in fractions of the basic width h = 1/12. We remark that the case r = 6, 3/16 h in Table IV corresponds to 25,025 mesh points, which is an upper limit in terms of core storage capacity on the CDC 6600 computer.

According to equation (2) the coefficients A_m and λ_m should be independent of which row we use in our tables. Our calculations confirm this and we obtain

$$A_o = 1.9 , \quad \lambda_o = 1.6 ,$$

$$A_1 = 2.3 , \quad \lambda_1 = 2.4 .$$

The agreement of λ_m with our estimates is correct to two significant digits.

We remark that the axially symmetric jet is expected to converge with r much faster because of the relative sizes of λ_1 and λ_o. Our calculations confirm this behavior. Using

equation (2), the correction for a jet corresponding to r = 4.5 is in the fifth decimal place. This is why we only had to take r = 4.5 for the axially symmetric model, whereas for the plane jet a calculation for r = 6 was required.

For the extrapolation with h, we observe that appreciable refinement of the mesh is necessary for the term Mh^2 to dominate the error as $h \to 0$. In Table V, calculations show that the convergence is $O(h^2)$ for the h/8 mesh (r = 1.5) and for the 3/16 h mesh (r = 3.75). For the jet lengths corresponding to r = 3 and r = 4.5, where the most refined mesh was only h/4, we find that there are contributions to the error from higher order terms. The same effect is present in the plane model, where we had to go to a 3/16 h mesh (r = 6) to verify that the convergence is $O(h^2)$.

Calculations using the extrapolation formula (2) give the final estimates

$$C_o = .61100$$

$$C_1 = .59135$$

The value of C_o is in error by only 2 units in the fifth decimal place. Close analysis of the data leads us to conclude that the error tolerance in the value of C_1 is $\pm.00004$.

5.2.3. Drag Coefficient

The drag coefficient $C_D(\sigma)$ was computed from the finite difference solution of the Riabouchinsky model by the formula

$$C_D(\sigma) = (1+\sigma)\left[1 + (1+m)/(q_o^2 y_o^{1+m}) \int_0^{K'} [\psi_u^2/(y^m y_v)]_{u+K}\, dv\right]$$

which is easily derived from the basic definition of C_D. In this formula σ is the cavitation parameter, q_o is the computed speed along the free boundary, y_o is the height of the plate, m is 0 or 1 for the plane or axially symmetric case, respectively, and the integration is carried out along the vertical side of the rectangle which maps onto the obstacle according to Simpson's Rule.

As with the vena contracta model, we calculated $\sigma(r,h)$ and $C_D(r,h)$ for various values of the rectangle length-to-width ratio $r = K/K'$ and for the three levels of mesh refinement h, h/2, h/4, where $h = K'/12$ (i.e. 12 intervals in the vertical direction). The results of the computations are shown in Tables VI and VII for the plane and axially symmetric cases, respectively.

For the plane case, extrapolation with h yields the data shown in the next to last row of Table VI. By comparison with the last row of the Table, which shows the exact values of σ and $C_D/1+\sigma$ for the given values of r, we see that our computations are accurate to about 4 significant figures. The maximum value 13/6 for r, corresponding to σ(exact) = .305355 represents an upper limit on r in terms of convergence, for we found that for larger values the scheme diverged. This divergence, which of course occurs also in the axially symmetric case, is the inevitable consequence of the rapidly increasing ratio

of cavity length to obstacle length caused by using the Riabouchinsky model to approximate Helmholtz flow. The free streamlines for Helmholtz flow actually have a parabolic shape at large distance from the obstacle.

For the axially symmetric case, extrapolation with h yields the data shown in the last row of Table VII. We estimate the accuracy to be comparable to that obtained in the plane case. The value r = 25/12 is an upper limit for convergence of the scheme. The results are plotted as a graph in Figure 5.4. We observe that the graph is remarkably linear in the range $.08 \leq \sigma \leq .6$ and that for smaller σ there is an indication of flattening of the curve. This qualitatively supports the theory [5] for the axially symmetric model which states that the asymptotic variation of $C_D/1+\sigma$ is $o(\sigma)$. Furthermore, extrapolation to $\sigma = 0$ yields, to 3 significant digits, the result

$$C_D(0) = .828 ,$$

which is in good agreement with the estimate stated in [5],

$$C_D(0) = .827 .$$

Finally we remark that our results are reasonably placed on the graph of experimental data available in the physically significant range $.1 \leq \sigma \leq .3$.

5.3. Conformal Mapping

As stated in Section 3.2, the method of steepest descent applied to the minimization of the Dirichlet-Douglas functional provides a numerical technique for obtaining conformal mappings.

In this case, a 3-point condition is specified and only tangential shifts are applied. In the course of our investigation of the more difficult free boundary problem, we conducted experiments using the conformal technique alone. The results are fragmentary, but they indicate that the method can be applied quite successfully.

We compute the analytic function which maps the rectangle R conformally onto the physical domain D_z as shown in Figure 5.5.

The following remarks are pertinent:

1) The rectangle R is fixed as shown in the w-plane. The image domain D_z consists of the part of the first quadrant bounded by the segment $x = b$, $0 \leq y \leq a$, an arc of the circle $x^2 + (y-b)^2 = a^2$, and appropriate segments of the coordinate axes.

2) The 3-point condition is given for the corners of the rectangle labelled A, C, and D. In particular the point D is mapped into ∞ in the z-plane. The corner B is free to move along the boundary of D_z between the points of A and C.

3) The point at infinity is not treated by subtraction of the pole at D. Instead, the problem is solved in the inverted domain given by

$$Z = 1/z \ ,$$

which maps the point at ∞ into the origin.

4) The formulation of the equations follow directly from the theory so we shall not bother to write them down. We note two

features. First, a pasting recipe is required, as it is for the cusped geometry model, to keep the images on the circular arc. Secondly, the corner B was treated in the same way as other points on the boundary according to the tangential shift formula.

5) Table VIII summarizes the results of the computations. For these runs the following quantities were used:

h - the basic mesh width = 1/12

r - the fixed length-to-width ratio of R = 1.5

α - the dissipation factor for the interior equations = 1.1

β - the tangential convergence factor on the boundary = 1.0

a - (see Figure 5.5) = .864440

b - (see Figure 5.5) = .4 and .8

The global difference between the solutions for the two values of b is that for b = .8, the image of the corner B lies on the vertical segment and for b = .4, it lies on the circular arc. The data verifies that the convergence of the numerical solution is $O(h^2)$.

Bibliography

[1] Garabedian, P. R., Partial Differential Equations, Wiley, New York, 1964.

[2] Milne-Thomson, L. M., Theoretical Hydrodynamics, 4th ed., Macmillan, New York, 1960.

[3] Garabedian, P. R. and Spencer, D. C., Extremal Methods in Cavitational Flow, J. Rat. Mech. Analysis 1, 1952.

[4] Byrd, P. F. and Friedman, M. D., Handbook of Elliptic Integrals for Engineers and Physicists, Springer, New York, 1964.

[5] Garabedian, P. R., Calculation of Axially Symmetric Jets and Cavities, Pacific J. Math. 6, 1956.

[6] Southwell, R. and Vaisey, G., Fluid Motions Characterized by "Free" Streamlines, Phil. Trans. Roy. Soc. London, Ser. A 240, 1948.

[7] Young, D., Gates, L., Arms, R. and Eliezer, D., The Computation of an Axially Symmetric Free Boundary Problem on NORC, U.S. Naval Proving Ground Rep. No. 1413, 1955.

[8] Cryer, C. W., On the Approximate Solution of One-Phase Free Boundary Problems in Two Dimensions, Mathematics Research Center, U.S. Army, Univ. of Wisconsin, M.R.C. Tech. Summary Rep. No. 894, 1968.

[9] Dowd, R. E., Asymptotic Description of the Cusps of a Hydrodynamic Figure of Equilibrium, N.Y.U., Courant Institute Rep. NYO-10435, 1964.

[10] Courant, R., Dirichlet's Principle, Interscience, New York, 1950.

[11] Garabedian, P. R., Estimation of the Relaxation Factor for Small Mesh Size, Math. Tables Aids Comp. 10, 1956.

[12] Bateman, H., Partial Differential Equations of Mathematical Physics, Cambridge, 1959.

[13] Trefftz, E., Über Die Kontraktion Kreisförmiger Flüssigkeitsstrahlen, Z. Math. Phys. 64, 1916.

[14] Hunt, B. W., Numerical Solution of an Integral Equation for Flow from a Circular Orifice, J. of Fluid Mech. 31, 1968.

[15] Gilbarg, D., Jets and Cavities, Encyclopedia of Physics 9, Springer-Verlag, 1960.

[16] Whittaker, E. T. and Watson, G. N., A Course in Modern Analysis, 4th ed., Cambridge, 1963.

Table I

Cusped Geometry Model

Rectangle length $a = \pi/2$ Basic mesh width $h = \pi/56$

Rectangle height $b = 3\pi/14$ Convergence parameters $\alpha = 2.2$

Coil radius $r = .510075$ $\beta = .9$

Wall constraint $\ell = .97$ $\gamma = .45$

Mesh width	Number of equations	Number of iterations	Separation points S_1, S_2	Midpoint M	λ^2
h	377	1210	.24134	.72657	1.20279
h/2	1425	2121	.21851	.72093	1.15358
h/4	5537	4187	.22031	.71946	1.14127
h/8	21825	8149	.21369	.71888	1.13635

Table II

Data for Specific Models (Figures 5.2 and 5.3)

Model	r	h	Number of equations	Number of iterations	α	β	γ	δ	n_e	n'_e	ℓ_c	ε
Vena Contracta plane	6	1/48	14161	6260	1.7	.1	.04	.1	120	2	24	.1
ax. sym.	4.5	1/48	10633	13368	6.0	.05	.02	.05	80	2	24	.1
Riabouchinsky plane	1.5	1/48	3577	1345	1.6	.4	.4	.8	52	2	16	.02
ax. sym.	1.5	1/48	3577	3992	1.0	.2	.2	.8	52	2	16	.02

Table III

Convergence of Discrete Solutions for r = 1.5, h = 1/12

ℓ and ℓ_u are the x-coordinate and u-derivative of the point M (Figs. 4.4 and 2.3) on the vertical line of symmetry. They are typical data points used to demonstrate second order convergence

Mesh width	Number of equations	Axially Symmetric Vena Contracta			Plane Riabouchinsky (exact values are ℓ=0, ℓ_u=.93065)		
		iterations	ℓ	ℓ_u	iterations	ℓ	ℓ_u
h	247	504	.634507	-.69967	1078	.004458	.92260
h/2	925	1169	.625442	-.69225	1110	.001069	.92902
h/4	3577	2574	.622734	-.69047	1345	.000271	.93028
h/8	14065	4925	.622022	-.69003	2239	.000069	.93056

Table IV

Contraction Coefficient $C_o(r,h)$ - Plane Jet

mesh h=1/12	r = 1.5	r = 3	r = 4.5	r = 6	mesh h=1/12	r = 6
h	.75506	.63442	.62245	.62150	3/4 h	.61412
h/2	.74891	.62637	.61387	.61271	3/8 h	.61177
h/4	.74817	.62521	.61265	.61146	3/16 h	.61129

Table V

Contraction Coefficient $C_1(r,h)$ - Axially Symmetric Jet

mesh h=1/12	r = 1.5	r = 3	r = 4.5	mesh h=1/12	r = 3.75
h	.66872	.60812	.60698	3/2 h	.60004
h/2	.65826	.59554	.59389	3/4 h	.59520
h/4	.65662	.59364	.59193	3/8 h	.59258
h/8	.65629	---	---	3/16 h	.59189

Table VI

Drag Coefficient - Plane Case

mesh	r=3/2		r = 5/3		r=11/6		r=2		r=13/6	
h=1/12	σ	$C_D/(1+\sigma)$	σ	$C_D/(1+\sigma)$	σ	$C_D/(1+\sigma)$	σ	$C_D/(1+\sigma)$	σ	$C_D/(1+\sigma)$
h	1.144427	.890126	.797988	.887302	.565171	.883661	.405063	.879054	.290195	.871239
h/2	1.150686	.888635	.798974	.885376	.568299	.882842	.411410	.880675	.301003	.878137
h/4	1.153172	.888458	.799649	.885053	.569502	.882843	.413447	.881359	.304184	.880149
extrap	1.154001	.888399	.799874	.884945	.569903	.882843	.414126	.881587	.305244	.880820
exact	1.154154	.888428	.799940	.884966	.569982	.882880	.414214	.881632	.305355	.880888

Table VII

Drag Coefficient - Axially Symmetric Case

mesh	r=4/3		r=17/12		r=3/2		r=19/12			
h=1/12	σ	$C_D/(1+\sigma)$	σ	$C_D/(1+\sigma)$	σ	$C_D/(1+\sigma)$	σ	$C_D/(1+\sigma)$	σ	$C_D/(1+\sigma)$
h	.570727	.851907	.439000	.848239	.339070	.845133	.262190	.842350	.202372	.839654
h/2	.579120	.844583	.447322	.840918	.347791	.838006	.271598	.835620	.212644	.833575
h/4	.581209	.843110	.449273	.839486	.349765	.836689	.273712	.834522	.214947	.832800
extrap	.5819	.84262	.4499	.83901	.3505	.83625	.2744	.83416	.2157	.83254

mesh	r=11/6		r=2		r=25/12	
h=1/12	σ	$C_D/(1+\sigma)$	σ	$C_D/(1+\sigma)$	σ	$C_D/(1+\sigma)$
h	.119772	.835753	.068415	.832021	.067258	.821411
h/2	.131182	.830819	.080798	.828905	.066638	.826531
h/4	.133557	.830515	.083309	.829129	.066470	.828273
extrap	.1344	.83042	.0841	.82920	.0664	.82885

Table VIII

Conformal Mapping Model - Convergence for

$r = 1.5$, $h = 1/12$

Mesh	Number of equations	Number of iterations		Image of the corner B (Figure 5.4)	
		b=.8	b=.4	b=.8	b=.4
h	247	458	414	.86444 + .73137i	.85523 + .52584i
h/2	925	1059	862	.86444 + .72264i	.85565 + .52297i
h/4	3577	2267	1812	.86444 + .72048i	.85575 + .52227i
h/8	14065	4807	3810	.86444 + .71994i	.85578 + .52209i

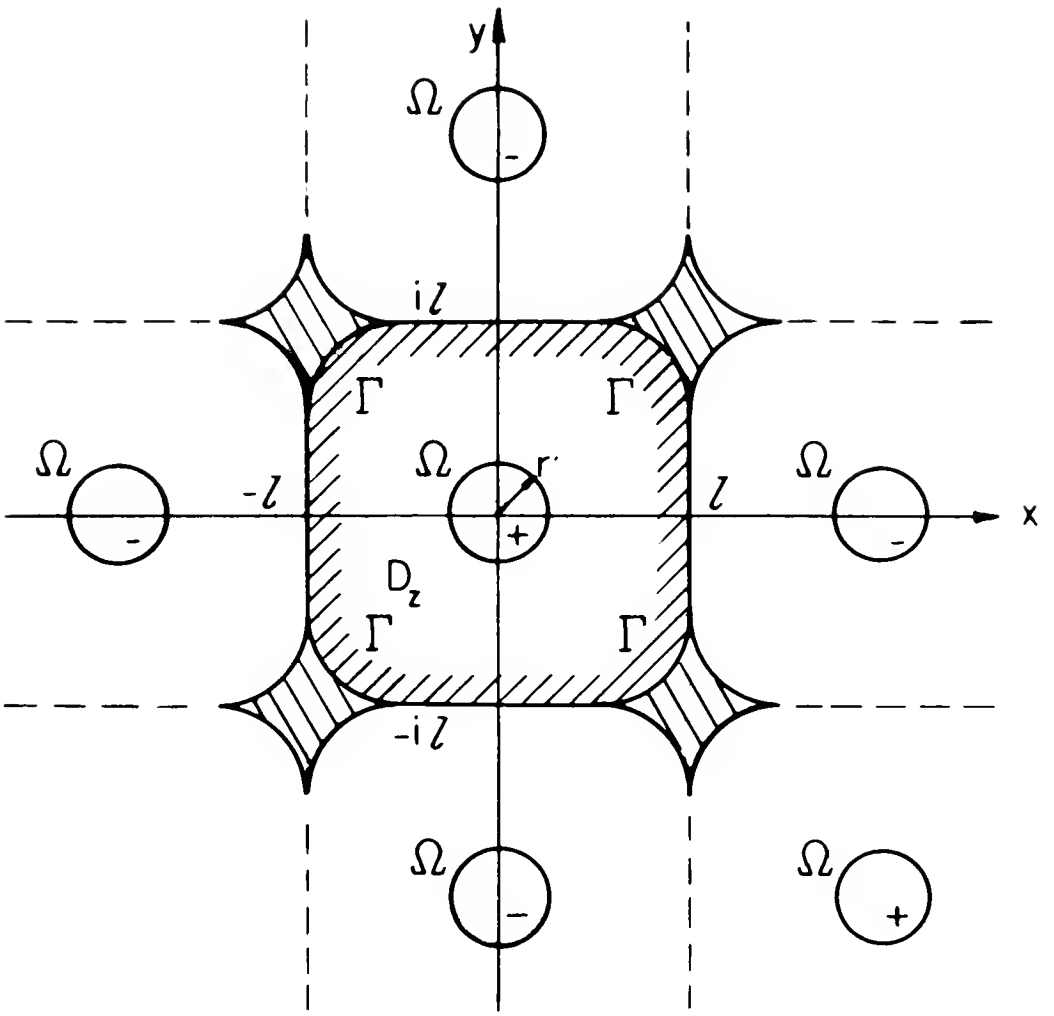

Figure 2.1 Cusped Geometry Model

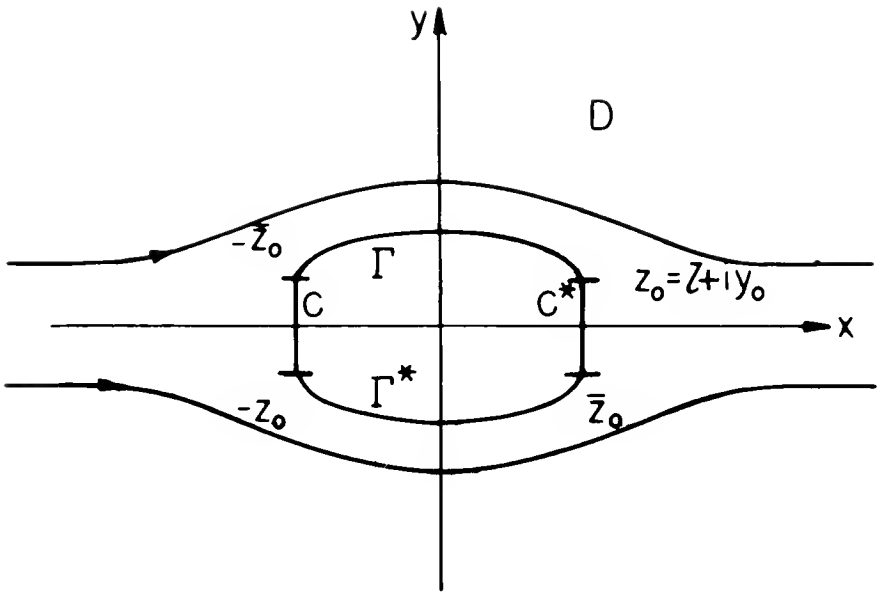

Figure 2.2 Riabouchinsky Flow

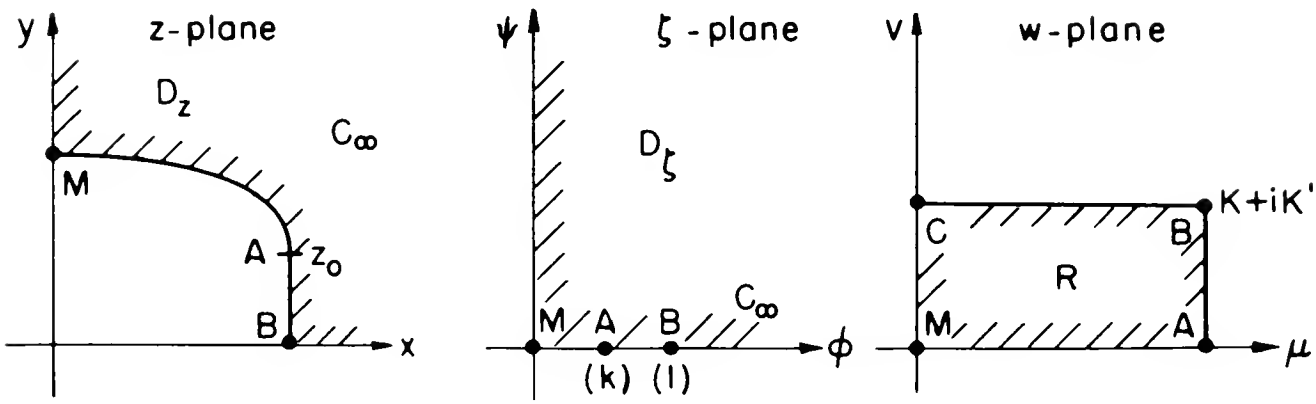

$(k = 1/(1+\alpha^2)^{1/2})$

(a) (b) (c)

Figure 2.3 Boundary Correspondance for Riabouchinsky Model

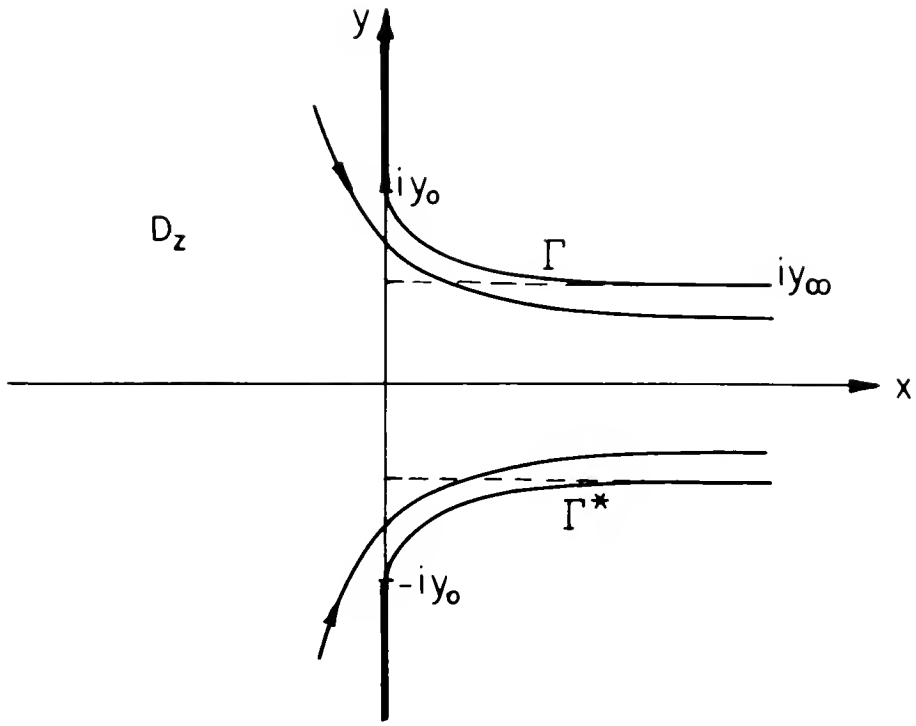

Figure 2.4 Vena Contracta Flow

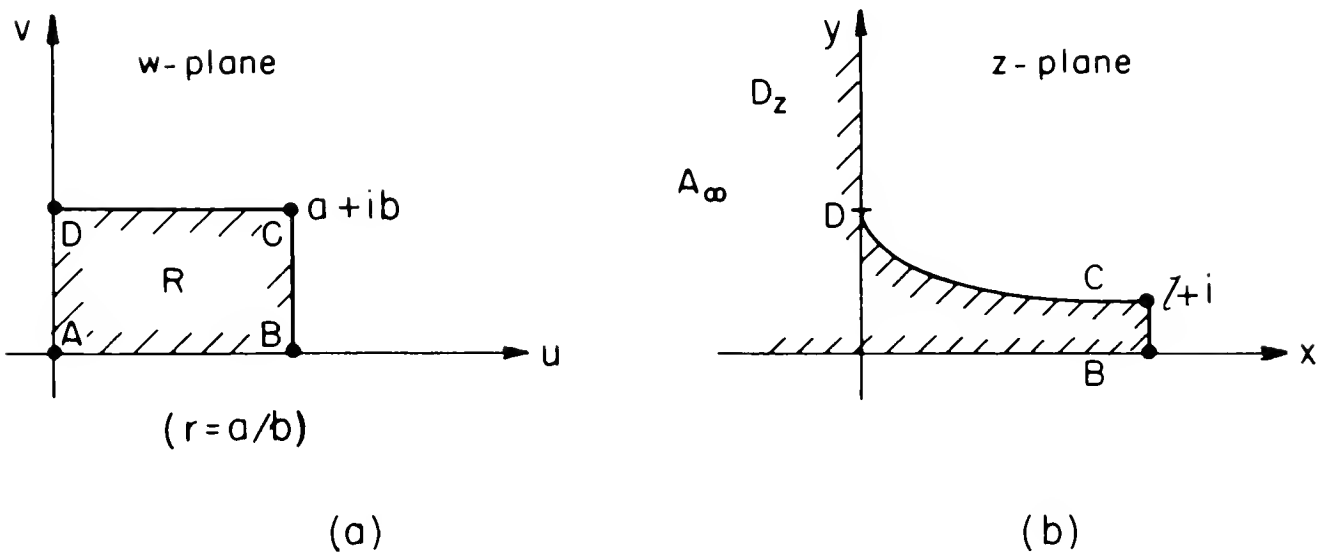

Figure 2.5

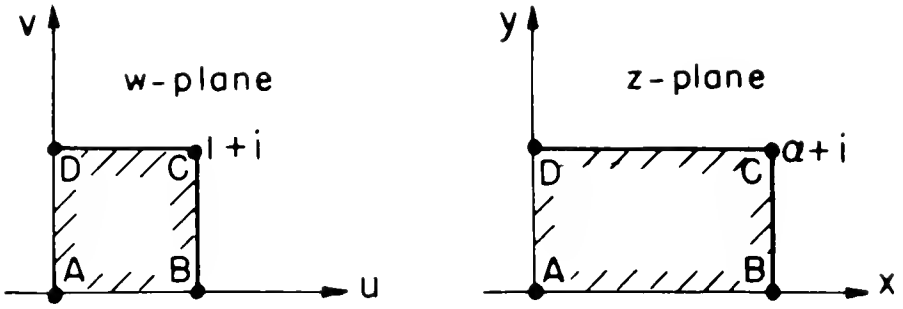

Figure 3.1 Rectangle Mapping

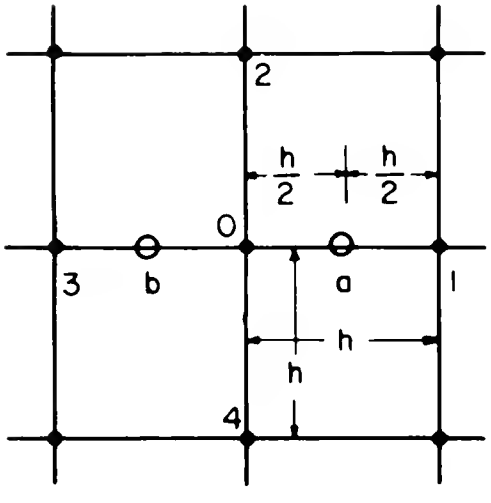

Figure 4.1

Finite Difference Equation for Axially-Symmetric ψ

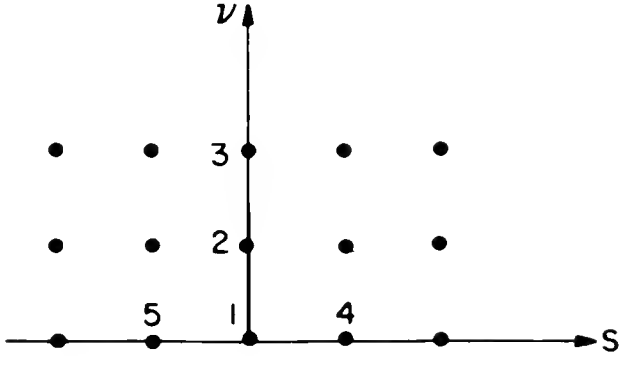

Figure 4.2

Finite Difference Equations at the Boundary

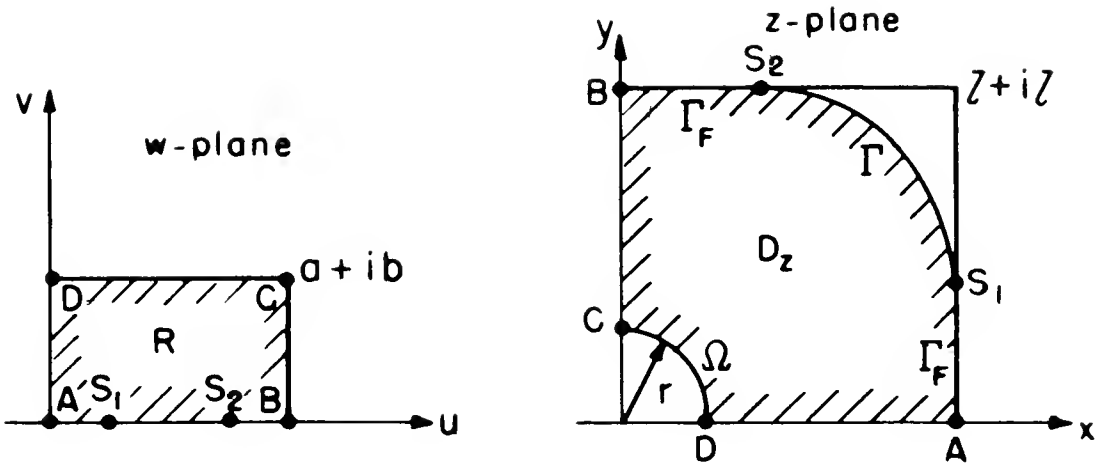

Figure 4.3 Cusped Geometry Conformal Mapping

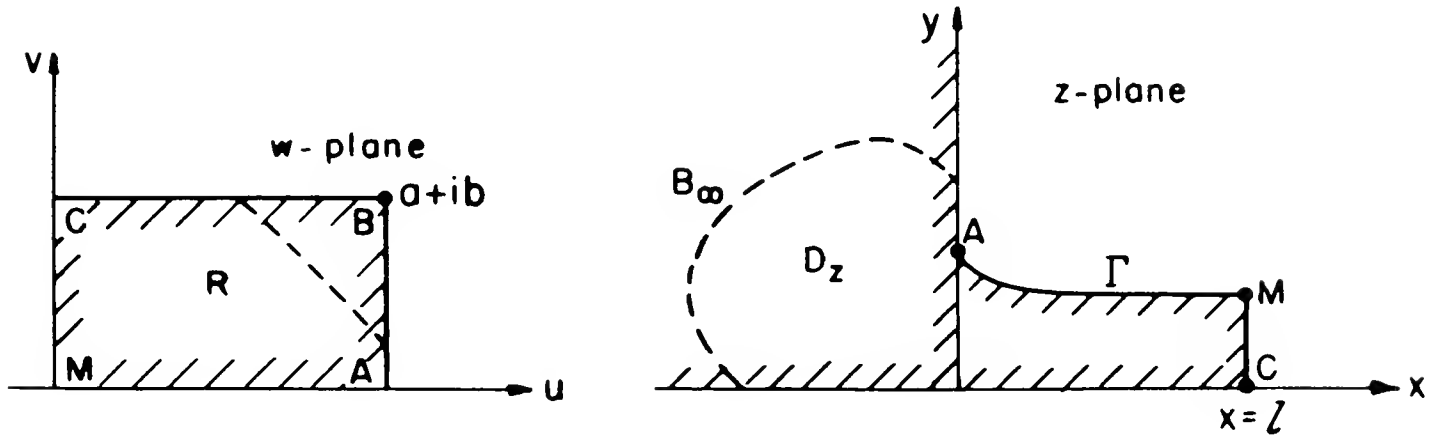

Figure 4.4 Vena Contracta Model Conformal Mapping

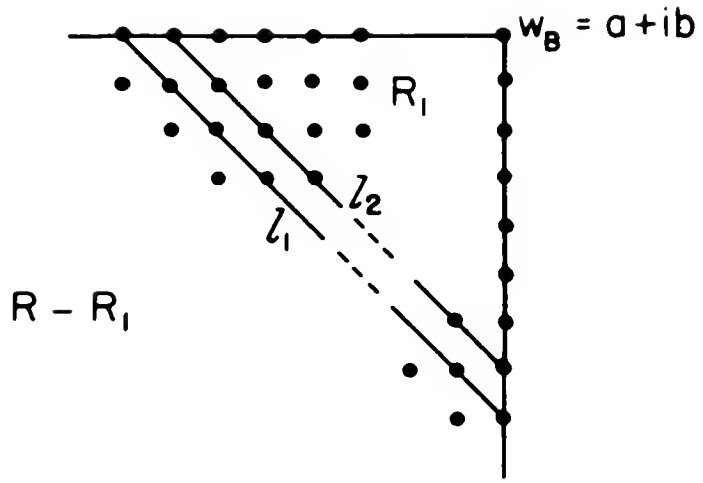

Figure 4.5 Interface Geometry

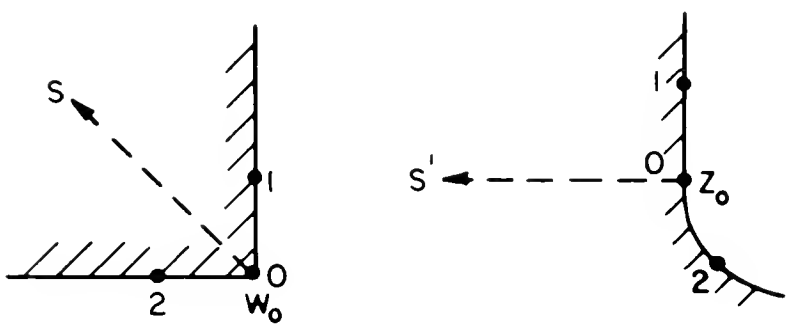

Figure 4.6 Treatment of the Separation Point

Cusped Geometry Model

$h = \frac{1}{4}\left(\frac{\pi}{28}\right)$

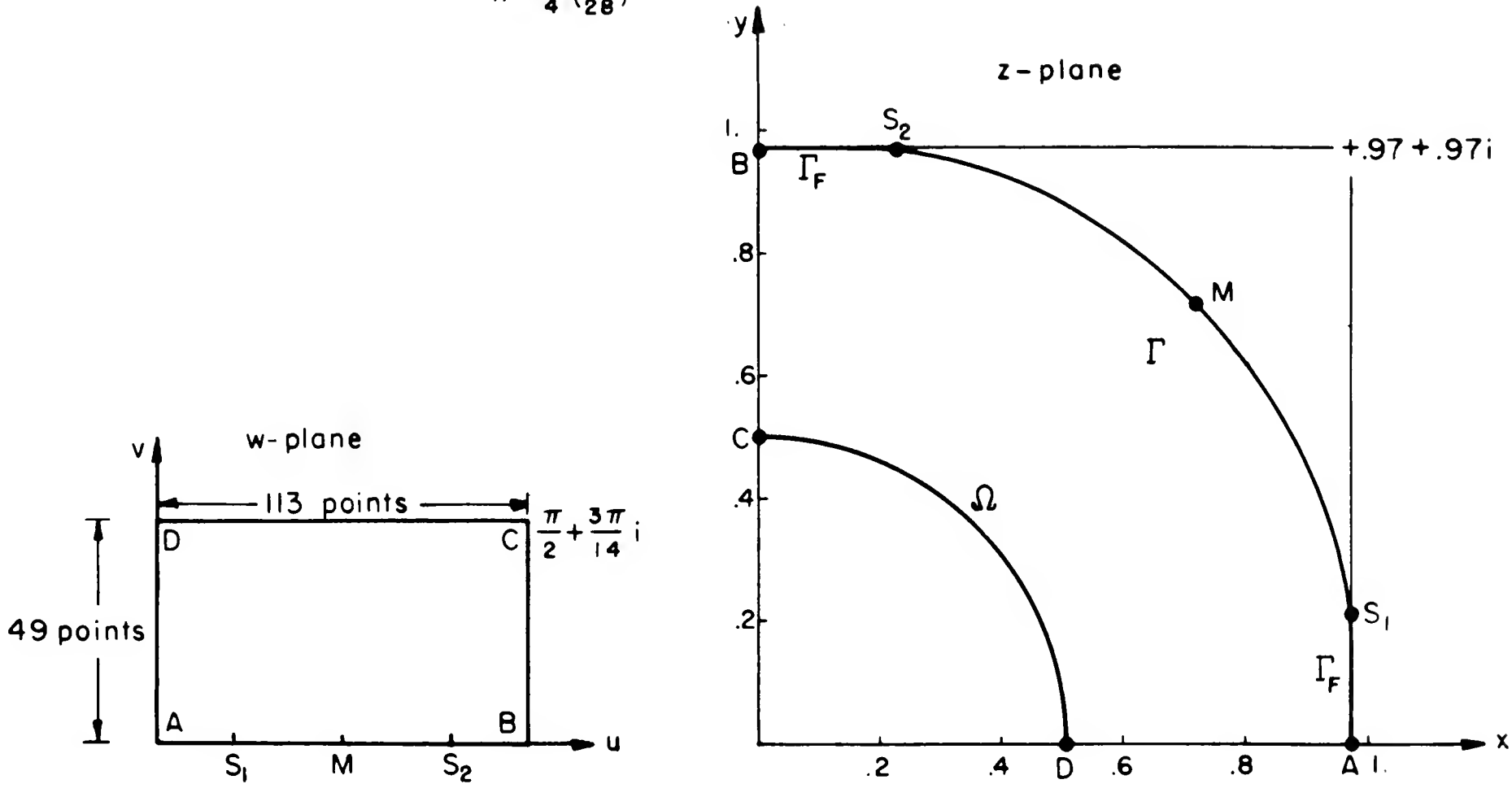

Figure 5.1

Vena Contracta Model

m = 0 Plane (computed and exact)
m = 1 Axially symmetric (computed)

	r	h	No. of Equations	Coordinates of M (Figure 4.4)	
				x	y
m = 0	6	1/48	14161	3.279	.611
m = 1	4.5	1/48	10633	2.900	.769

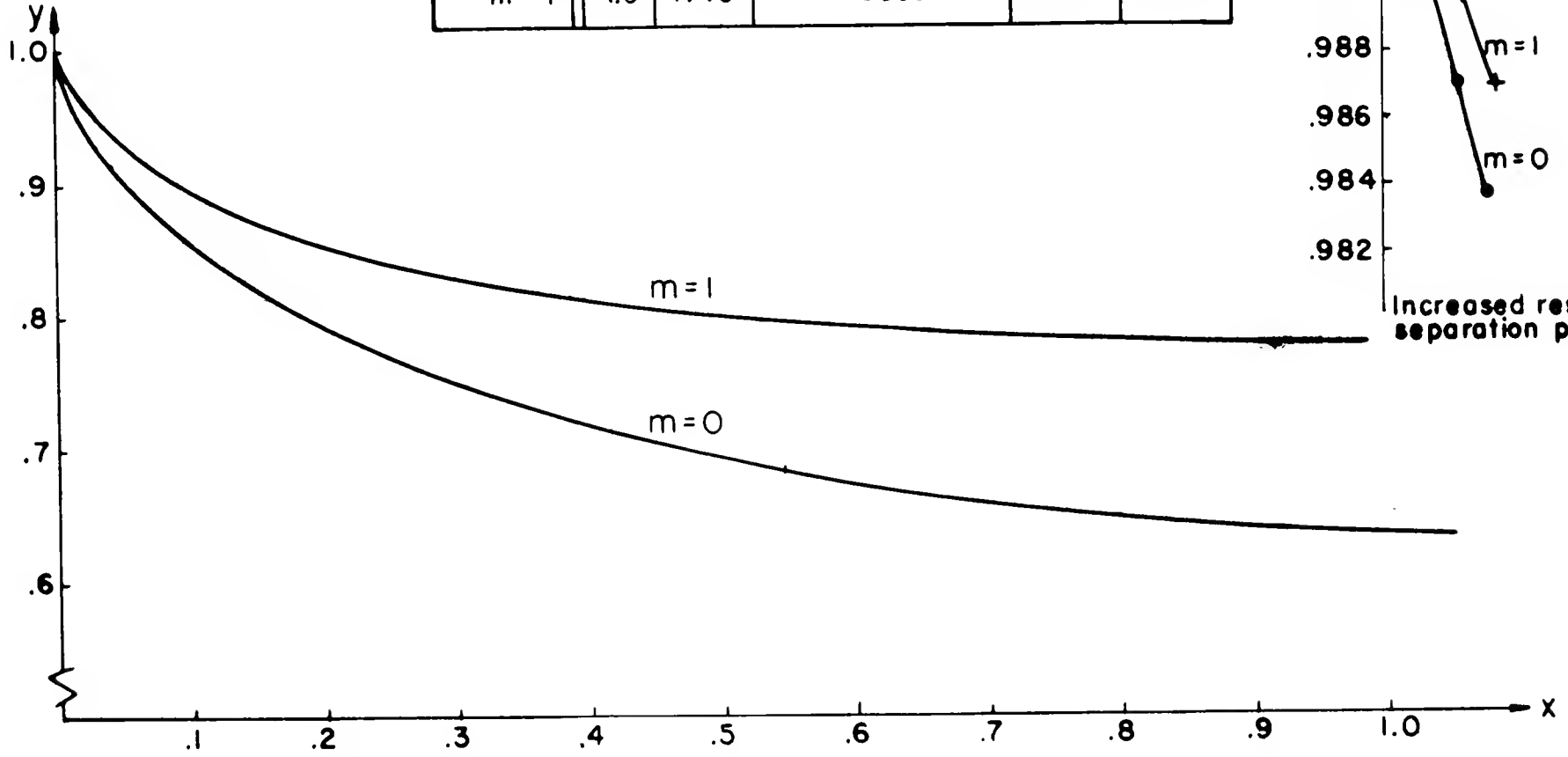

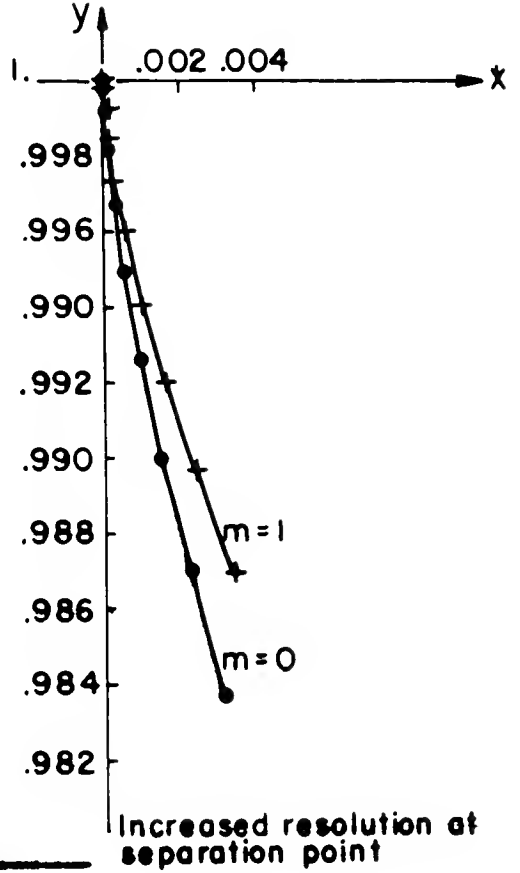

Figure 5.2

Riabouchinsky Model

m=0 Plane (computed and exact)
m=1 Axially symmetric (computed)

	r	h	No. of Equations	Coordinates of midpoint M	
				x	y
m = 0	1.5	K'/48	3577	.000	.509
m = 1	1.5	K'/48	3577	-.055	.494

Separation point z_0 = .86444 + .25886

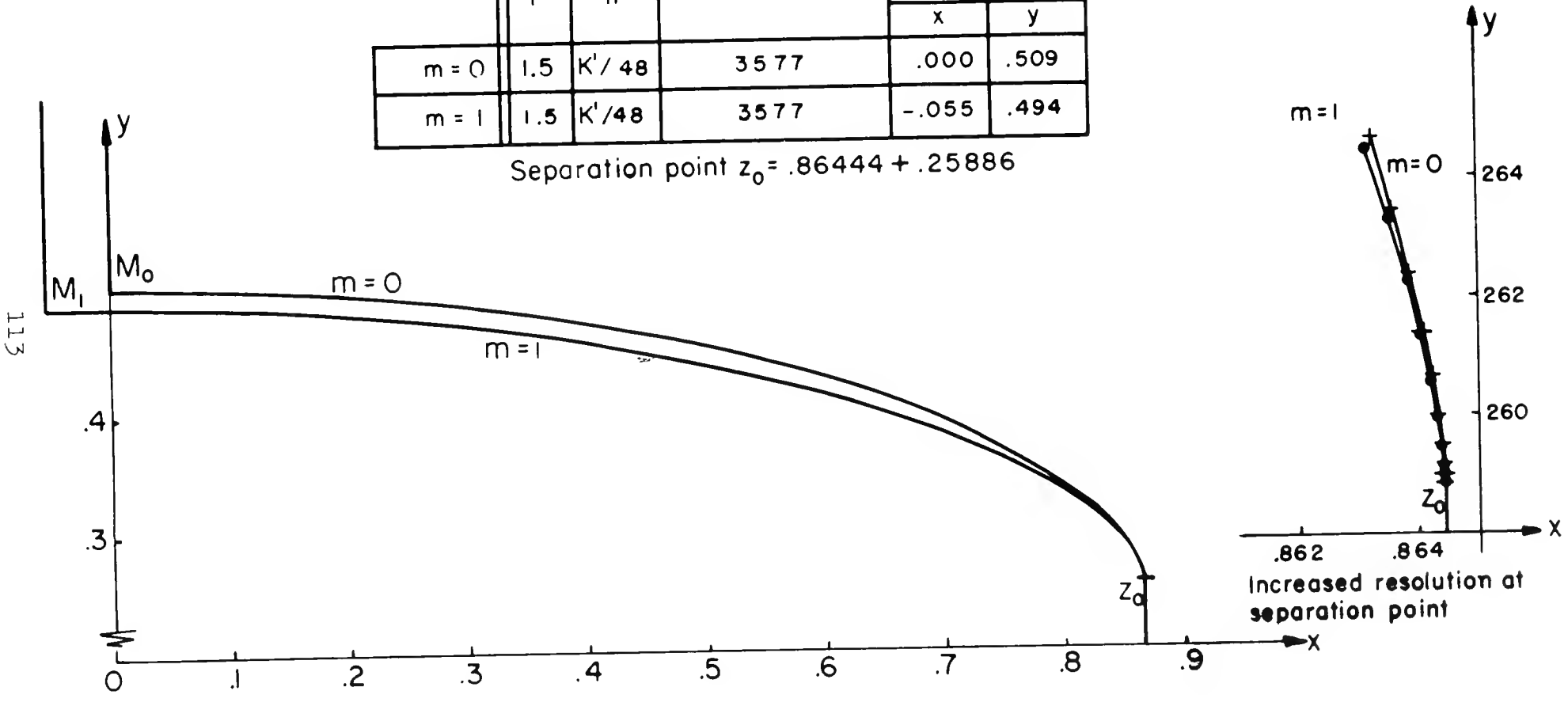

Figure 5.3

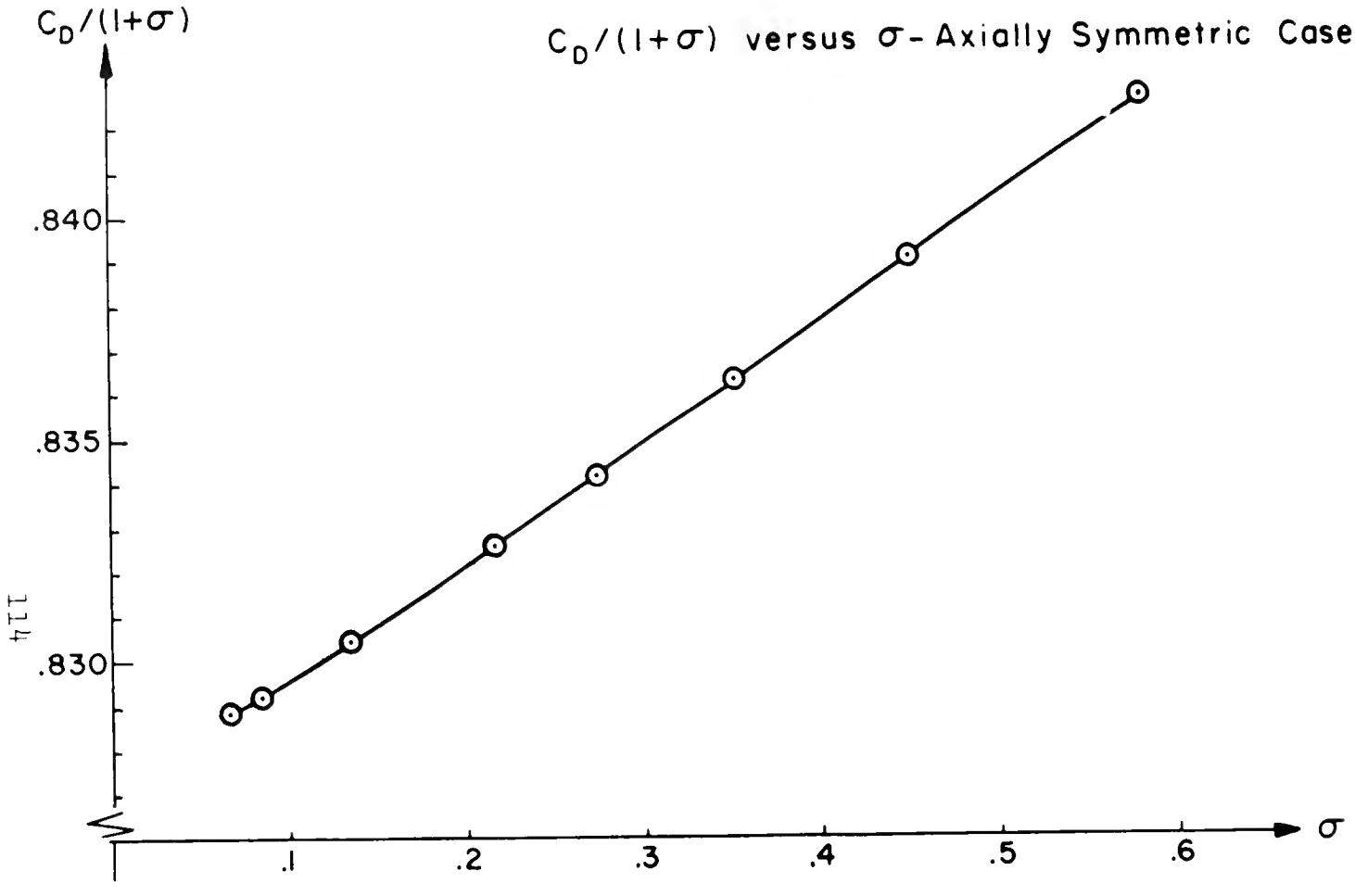
$C_D/(1+\sigma)$
$C_D/(1+\sigma)$ versus σ - Axially Symmetric Case
.840
.835
.830
.1
.2
.3
.4
.5
.6
σ

Figure 5.4

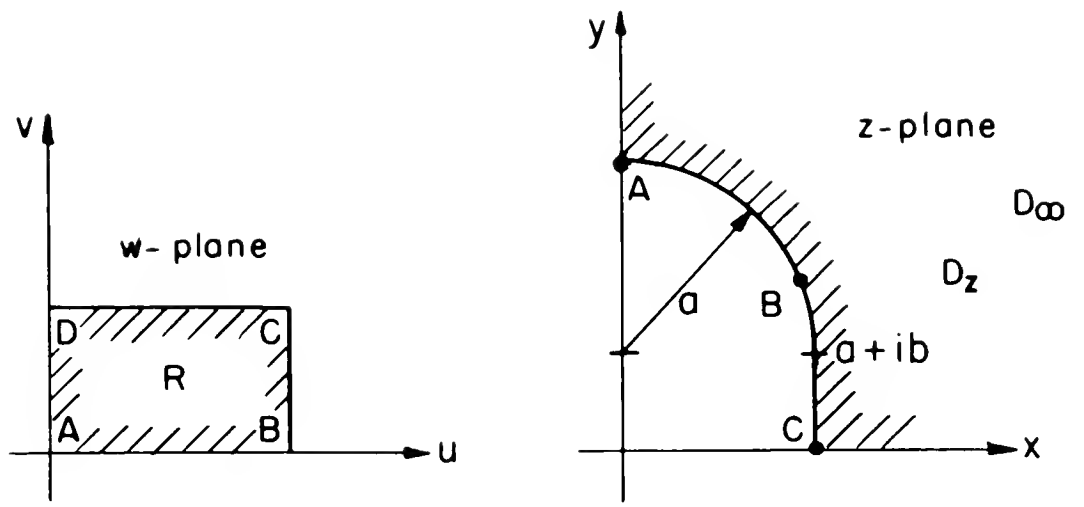

Figure 5.5 Conformal Mapping Model

Appendix B

On the following pages is given the Fortran IV program for the Riabouchinsky model as coded for the CDC 6600 computer at New York University. Also included is actual output for an axially symmetric run corresponding to $r = 1.5$, $h = K'/12$. This case is set by the parameters

$$NH = 18$$

$$NV = 12$$

on the data card. Also input on this data card (Format 14 of the code) are the various convergence parameters and control devices, each of which can be deciphered by close study of the code and the output.

```
      PROGRAM RIAB(INPUT,OUTPUT,RIAB109,TAPE 1=RIAB109)
      COMMON/B1/ADV,BDV,CDV,X0,NV,NH,NV1,NH1,NTOT,NC,SR1,CA,SRI,H,NIT
      COMMON/B2/XKL,XKLP,XK,XKP,E,EP,Q,QP,IS1,IS2
     1,MD1,MD2,MD3,MD4,AVG1,AVG2,AMAX,BMAX,CMAX,MAXA,MAXB,MAXC,B1,B2,B3,
     2SR,I,ERLIM,HLENGH,UINF,IP,NE,NEP,NL,EPS,ZB(225),ZS(100),
     3UD(225),VD(225),PSIV(225),CON(50),  X( 2000) ,Y( 2000),PSI( 2000)
      COMPLEX ZB,ZS,Z1,Z2,UD,VD
C*** READ IN AND SET INITIAL PARAMETERS
      PI=3.14159265358979
   23 READ 14,NH,NV,NIT,MD1,MD2,MD3,MD4,NC,NL,NE,NEP,IP,IS1,IS2,
     XCON(1),CON(2),CON(3),CON(4),EPS
   14 FORMAT(2I3,I5,4I1,7I2,5F5.0)
      IF(NH.LT.0) CALL EXIT
      I=0             $IP1=500             $ITR=0              $NC=NC*NV/12
      NE=NE*NV/12  $NL=(NL-1)*NV/12+1  $IS2=IS2*NV/12        $NITP=5*NH
      Q=EXP(-PI*NV/NH)                     $QP=EXP(-PI*NH/NV)  $XK=FK1(Q)
      XKP=XK*ALOG(1./Q)/PI                 $XKL=FXKL(XK,Q)     $XKL2=XKL**2
      XKLP=SQRT(1.-XKL2)                   $E=EE(PI/2.,XKL2)   $IS1=NIT/IS1
      EP=EE(PI/2.,1.-XKL2)                 $H=XK/NH            $NH1=NH+1
      NV1=NV+1       $NTOT=NH1*NV1         $SR=2./(1.+CON(4)*H)$SRI=1./SR
      SR1=1.-SR      $CA=.25*SR            $ADV=1.5/H          $BDV=-2./H
      CDV=.5/H       $B1=CON(1)*H          $B2=CON(2)*H        $B3=CON(3)*H
      HLENGH=(E-(1.-XKL2)*XK)/XKL          $UINF=XKL/(1.+XKLP) $ERLIM=1.E-6
C*** PRINT INITIAL DATA
      CALL SPEW(1)
      GO TO (27,11,98),MD2
C*** MD2=1 USE EXACT PLANE SOLUTION FOR INITIAL GUESS
   27 DO 21 L=1,NH1
      SN=SNF((L-1.)*H,Q,XK,XKL)
      CN =SQRT(AMAX1(0.,1.-SN **2))
      DN=SQRT(1.-(XKL*SN)**2)
      N1=1+(L-1)*NV1
      N2=N1+NV1
      DO 21 N=N1,N2
      IF(N.EQ.NV1) GO TO 21
      SNP=SNF((N-N1)*H,QP,XKP,XKLP)
      CNP=SQRT(AMAX1(0.,1.-SNP**2))
      DNP=SQRT(1.-(XKLP*SNP)**2)
      Z2=CMPLX((L-1.)*H,(N-N1)*H)
      Z1=(CMPLX(EF1(REAL(Z2),E,XK,Q),AIMAG(Z2)-EF1(AIMAG(Z2),EP,XKP,QP))
     X+(CMPLX(XKL2*SN*CN*DN*SNP**2,SNP*CNP*DNP*DN**2)+(0.,1.)*XKLP*(DN*
     XCNP*DNP-(0.,1.)*XKL2*SN*CN*SNP))/(CNP**2+XKL2*(SN*SNP)**2)-(1.-XKL
     X2)*Z2+CMPLX(0.,EP-XKL2*XKP))/XKL
      IF(N.GT.N1+(L-1)*(NV1+1)+1)  Z1=Z1-1./UINF/(Z2-XKP*(0.,1.))
      X(N)=REAL(Z1)
      Y(N)=AIMAG(Z1)
      IF(N.EQ.N2) Y(N)=0.
   21 CONTINUE
      X(NV1)=0.
      Y(NV1)=0.
      X0=1.
      GO TO 16
C*** MD2=2 INTERPOLATE PRESENT SOLUTION FOR INITIAL GUESS
   11 CALL READY(X,Y,ZB,ZS,NH1,NV1,NTOT,X0)
      GO TO 16
```

PAGE NO. 1

```
C*** MD2=3 USE BOUNDARY DATA STORED ON TAPE 1 FOR INITIAL GUESS
   98 REWIND 1
      READ (1) ZB,ZS,X0
      DO 97 N=1,NTOT
      X(N)=0.
   97 Y(N)=0.
      DO 96 L=1,NTOT,NV1
      Z1=ZB(1+L/NV1)
      X(L)=REAL(Z1)
   96 Y(L)=AIMAG(Z1)
      N1=NTOT-NV
      DO 95 L=N1,NTOT
      Z1=ZS(1+L-N1)
      X(L)=REAL(Z1)
   95 Y(L)=AIMAG(Z1)
      DO 99 L=1,NV1
   99 X(L)=X0
C*** SET UP INTERIOR INITIAL GUESS USING FIXED BOUNDARY DATA FROM
C     OPTIONS FOR MD2
   16 DO 17 L=1,NTOT
   17 PSI(L)=0.
      DO 42 L=1,NITP
   42 CALL ZCHUG(X,Y,PSI,XKP,MD4,(MD4+1)**2,UINF)
      IF(MD4.EQ.0) GO TO 43
      DO 41 L=1,NITP
   41 CALL ZCHUG(X,Y,PSI,XKP,MD4,1,UINF)
   43 DO 5 L=1,NH1
      N1=1+(L-1)*NV1
    5 ZB(L)=CMPLX(X(N1),Y(N1))
      DO 3 L=N1,NTOT
      K=L-N1+1
    3 ZS(K)=CMPLX(X(L),Y(L))
      IF(MD3.EQ.2)  GO TO 22
C*** PRINT INITIAL BOUNDARY VALUES AND DERIVATIVES
      CALL DERIV(UD,VD,PSIV,X,Y,PSI,ZB,ZS,1)
      CALL SPEW(3)
      CALL DERIV(UD,VD,PSIV,X,Y,PSI,ZB,ZS,2)
      CALL SPEW(4)
      CALL SPEW(9)
   22 CALL SPEW(2)
C*** BEGIN MAIN ITERATION SCHEME
      DO 7 I=1,NIT
C*** TRANSFER PRESENT BOUNDARY DATA FROM ZB, ZS TO X,Y
      DO 8 L=1,NTOT,NV1
      Z1=    ZB(1+L/NV1)
      X(L)=REAL(Z1)
    8 Y(L)=AIMAG(Z1)
      N1=NTOT-NV
      DO 9 L=N1,NTOT
      Z1=    ZS(1+L-N1)
      X(L)=REAL(Z1)
    9 Y(L)=AIMAG(Z1)
C*** ITERATE INTERIOR - TEXT EQUATIONS 4.13A-4.13C
      IF(I.EQ.IP1.OR.I.LE.500) ITR=1
      CALL ZCHUG(X,Y,PSI,XKP,MD4,ITR,UINF)
      IF(ITR.EQ.1.AND.I.GE.500) IP1=IP1+IP
```

PAGE NO. 2

```
      ITR=0
      AVG2=0.
      AMAX=0.
      BMAX=0.
      CMAX=0.
C*** ITERATE FIXED BOUNDARY - TEXT EQUATION 4.13D
      CALL DERIV(UD,VD,PSIV,X,Y,PSI,ZB,ZS,3)
      CALL EXTRAP(CON(5),XK,NEP,H,NV1,UD,PSIV,CON(3),CON(4),1,MD4,ZS)
      DO 10 L=2,NV1
      IF(MOD(I,IS2).EQ.0) CALL MAXVAL(CMAX,REAL(VD(L)/UD(L)),L,MAXC)
   10 ZS(L)=CMPLX(HLENGH,AIMAG(ZS(L))-B2*AIMAG(UD(L)))
      ZS(1)=ZS(1)+B2/SQRT(2.)*CMPLX(0.,AIMAG(VD(1))-AIMAG(UD(1)))
      ZB(NH1)=ZS(1)
      IF(MOD(I,IS1).EQ.0) CALL SPEW(3)
C*** ITERATE FREE BOUNDARY - TEXT EQUATION 4.13E
      CALL DERIV(UD,VD,PSIV,X,Y,PSI,ZB,ZS,2)
      CALL EXTRAP(CON(6),XK,NE,H,NH1,VD,PSIV,CON(1),CON(2),2,MD4,ZB)
      AVG1=(1.-EPS)*CON(6)+EPS*CON(5)
C*** CHECK FOR DIVERGENCE
      IF(100..LE.REAL(UD(1))+AIMAG(VD(1)).OR.Y(1).LE..1) GO TO 12
      DO 13 L=1,NH
      AVAL=REAL(UD(L)/VD(L))
      BVAL=(REAL(VD(L))**2+AIMAG(VD(L))**2)/PSIV(L)**2*AIMAG(ZB(L))**(2*
     XMD4)/AVG1-1.
      CALL MAXVAL(AMAX,AVAL,L,MAXA)
      IF(MOD(I,IS2).EQ.0) CALL MAXVAL(BMAX,BVAL,L,MAXB)
   13 ZB(L)=ZB(L)+B2 *AVAL*UD(L)+B3 *BVAL*VD(L)
C*** ITERATE L-SHIFT - TEXT EQUATION 4.13F
      DO 15 L=1,NL
      XV=REAL(VD(L)*CONJG(VD(L)))
      XU=REAL(UD(L)*CONJG(UD(L)))
   15 AVG2=AVG2+(XV-XU)/(XV+XU)
      AVG2=AVG2/NL
      X0=X0-B1*AVG2
      DO 28 N=1,NV1
   28 X(N)=X0
      ZB(1)=CMPLX(X0,AIMAG(ZB(1)))
C*** CHECK FOR CONVERGENCE
      IF(ABS(AMAX).GT.ERLIM) GO TO 30
      CALL SPEW(7)
      CALL SPEW(4)
      CALL DERIV(UD,VD,PSIV,X,Y,PSI,ZB,ZS,1)
      CALL SPEW(3)
      GO TO 20
   30 IF(MOD(I,IS1).EQ.0) CALL SPEW(4)
   24 IF(MOD(I,IS2).EQ.0) CALL SPEW(6)
      IF(MOD(I,500).NE.0 .OR. MD1.NE.2) GO TO 7
      REWIND 1
      WRITE (1) ZB,ZS,X0
    7 CONTINUE
   20 CALL SPEW(9)
      CALL SPEW(10)
      CALL SPEW(8)
      IF(MD1.NE.2) GO TO 23
      REWIND 1
      WRITE (1) ZB,ZS,X0
      GO TO 23
   12 CALL SPEW(4)
      CALL SPEW(5)
      GO TO 23
      END
```

PAGE NO. 3

```
      SUBROUTINE DERIV(UD,VD,PSIV,X,Y,PSI,ZB,ZS,K)
C*** COMPUTE DERIVATIVES ALONG FIXED BOUNDARY (K=1 OR 3) AND ALONG
C     FREE BOUNDARY (K=2)
      COMMON/B1/ADV,BDV,CDV,X0,NV,NH,NV1,NH1,NTOT,NC,SR1,CA,SRI,H,NIT
      COMPLEX UD,VD,ZB,ZS
      DIMENSION UD(1),VD(1),ZB(1),ZS(1),X(1),Y(1),PSI(1),PSIV(1)
      GO TO (1,2,1),K
    1 DO 3 L=1,NV1
      N1=NTOT-NV1+L
      UD(L)=ADV*ZS(L)+BDV*CMPLX(X(N1-NV1),Y(N1-NV1))+CDV*CMPLX(X(N1-2*NV
     11),Y(N1-2*NV1))
      IF(K.EQ.3) PSIV(L)=ADV*PSI(N1)+BDV*PSI(N1-NV1)+CDV*PSI(N1-2*NV1)
    3 VD(L)=CDV*(ZS(L+1)-ZS(L-1))
      VD(1)=(ZS(2)-ZS(1))*CDV*2.
      UD(1)=(ZS(1)-ZB(NH))*CDV*2.
      VD(NV1)=CDV*(CONJG(ZS(NV1-1))-ZS(NV1-1))
      RETURN
    2 DO 4 L=1,NH1
      N=1+ (L-1)*NV1
      VD(L)=-ADV*ZB(L)-BDV*CMPLX(X(N+1),Y(N+1))-CDV*CMPLX(X(N+2),Y(N+2))
      PSIV(L)=-ADV*PSI(N)-BDV*PSI(N+1)-CDV*PSI(N+2)
    4 UD(L)=CDV*(ZB(L+1)-ZB(L-1))
      UD(1)=CDV*(ZB(2)-CMPLX(2.*X0-REAL(ZB(2)),AIMAG(ZB(2))))
      UD(NH1)=(ZB(NH1)-ZB(NH))*CDV*2.
      VD(NH1)=(ZS(2)-ZS(1))*CDV*2.
      RETURN
      END


      SUBROUTINE FLIP(X,Y,P,K,RES,XKP,H,NC,NA,NV1,UINF,MD4,ITR)
C*** SET BOUNDARY CONDITIONS ALONG INTERFACE  K=-1 REGION R TO REGION R1
C                                             K=+1 REGION R1 TO REGION R
      DIMENSION X(1),Y(1),P(1)
      COMPLEX Z
      N1=NC
      N2=NC+1
      DO 1 L=1,NA
      IF(L.EQ.NA) N2=N1
      DO 2 N=N1,N2
      IF(ITR.EQ.1.AND.K.EQ.-1) P(N)=P(N)-UINF/(1.+MD4)*Y(N)**(1+MD4)
      Z= CMPLX(X(N),Y(N))+K*RES/CMPLX((L-1.)*H,(NC-2.+L+N-N1)*H-XKP)
      Y(N)=AIMAG(Z)
      IF(ITR.EQ.1.AND.K.EQ. 1) P(N)=P(N)+UINF/(1.+MD4)*Y(N)**(1+MD4)
    2 X(N)=REAL(Z)
      N1=N1+NV1+1
    1 N2=N1+1
      RETURN
      END


      SUBROUTINE MAXVAL(XMAX,XVAL,N,MAX)
C*** CALCULATION OF MAXIMUM BOUNDARY RESIDUALS
      IF(ABS(XVAL) .LT. ABS(XMAX))  RETURN
      XMAX=XVAL
      MAX=N
      RETURN
      END
```

PAGE NO. 4

```
      SUBROUTINE ZCHUG(X,Y,P,XKP,MD4,ITR,UINF)
C*** ITERATE INTERIOR     MD4=0 PLANE              ITR=0 DO NOT ITERATE PSI
C                         MD4=1 AXIAL SYMMETRY     ITR=1 ITERATE PSI
      COMMON/B1/ADV,BDV,CDV,X0,NV,NH,NV1,NH1,NTOT,NC,SR1,CA,SRI,H,NIT
      DIMENSION X(1),Y(1),P(1),Y1(2000)
      NA=NV1-NC $ NA1=NA+1 $ NA2=NA-1 $ N1=2 $ NC1=NC+1 $ RES=1./UINF
C*** ITERATE THROUGH REGION R
      DO 1 L=2,NC
      IF(ITR.EQ.0) GO TO 1
      IF(MD4.EQ.0) P(L)=SR1*P(L)+CA*(P(L+1)+P(L-1)+2.*P(L+NV1))
      IF(MD4.EQ.1) P(L)=SR1*P(L)+(P(L+1)/(Y(L)+Y(L+1))+P(L-1)/(Y(L)+Y(L-
     X1))+2.*P(L+NV1)/(Y(L)+Y(L+NV1)))/(SRI/(Y(L)+Y(L+1))+SRI/(Y(L)+Y(L-
     X1))+2.*SRI/(Y(L)+Y(L+NV1)))
    1 Y(L)=SR1*Y(L)+CA*(Y(L+1)+Y(L-1)+2.*Y(L+NV1))
      DO 10 L=2,NH
      N1=N1+NV1
      N2=MIN0(N1+NC-3+L,NV1*L-1)
      IF(ITR.EQ.0) GO TO 6
      IF(MD4.EQ.1) GO TO 7
      DO 8 N=N1,N2
    8 P(N)=SR1*P(N)+CA*(P(N+1)+P(N-1)+P(N+NV1)+P(N-NV1))
      GO TO 6
    7 DO 9 N=N1,N2
    9 P(N)=SR1*P(N)+(P(N+1)/(Y(N)+Y(N+1))+P(N-1)/(Y(N)+Y(N-1))+P(N+NV1)/
     X(Y(N)+Y(N+NV1))+P(N-NV1)/(Y(N)+Y(N-NV1)))/(SRI/(Y(N)+Y(N+1))+SRI/(
     XY(N)+Y(N-1))+SRI/(Y(N)+Y(N+NV1))+SRI/(Y(N)+Y(N-NV1)))
    6 DO 11 N=N1,N2
      X(N)=SR1*X(N)+CA*(X(N+1)+X(N-1)+X(N+NV1)+X(N-NV1))
   11 Y(N)=SR1*Y(N)+CA*(Y(N+1)+Y(N-1)+Y(N+NV1)+Y(N-NV1))
      IF(L.LE.NA) GO TO 10
      N=N2+1
      X(N)=SR1*X(N)+CA*(2.*X(N-1)+X(N+NV1)+X(N-NV1))
   10 CONTINUE
C***  CROSSOVER TO REGION R1
      CALL FLIP(X,Y,P,-1,RES,XKP,H,NC,NA1,NV1,UINF,MD4,ITR)
      IF(ITR.EQ.1.AND.MD4.EQ.1) CALL CROSS( 1,X,Y,Y1,P,RES,H,XKP,NV,NA1,
     XNA2,NC,NV1)
C*** ITERATE THROUGH REGION R1
      DO 13 L=NC1,NV
      IF(ITR.EQ.0) GO TO 13
      IF(MD4.EQ.0) P(L)=SR1*P(L)+CA*(P(L+1)+P(L-1)+2.*P(L+NV1))
      IF(MD4.EQ.1) P(L)=SR1*P(L)+(P(L+1)/(Y1(L)+Y1(L+1))+P(L-1)/(Y1(L)+Y
     X1(L-1))+2.*P(L+NV1)/(Y1(L)+Y1(L+NV1)))/(SRI/(Y1(L)+Y1(L+1))+SRI/(Y
     X1(L)+Y1(L-1))+2.*SRI/(Y1(L)+Y1(L+NV1)))
   13 Y(L)=SR1*Y(L)+CA*(Y(L+1)+Y(L-1)+2.*Y(L+NV1))
      N2=NV
      N1=NC1
      DO 14 L=2,NA2
      N1=N1+NV1+1
      N2=N2+NV1
      IF(ITR.EQ.0) GO TO 15
      IF(MD4.EQ.1) GO TO 16
      DO 17 N=N1,N2
   17 P(N)=SR1*P(N)+CA*(P(N+1)+P(N-1)+P(N+NV1)+P(N-NV1))
      GO TO 15
```

PAGE NO. 5

```
   16 DO 18 N=N1,N2
   18 P(N)=SR1*P(N)+(P(N+1)/(Y1(N)+Y1(N+1))+P(N-1)/(Y1(N)+Y1(N-1))+P(N+N
     XV1)/(Y1(N)+Y1(N+NV1))+P(N-NV1)/(Y1(N)+Y1(N-NV1)))/(SRI/(Y1(N)+Y1(N
     X+1))+SRI/(Y1(N)+Y1(N-1))+SRI/(Y1(N)+Y1(N+NV1))+SRI/(Y1(N)+Y1(N-NV1
     X)))
   15 DO 19 N=N1,N2
      X(N)=SR1*X(N)+CA*(X(N+1)+X(N-1)+X(N+NV1)+X(N-NV1))
   19 Y(N)=SR1*Y(N)+CA*(Y(N+1)+Y(N-1)+Y(N+NV1)+Y(N-NV1))
      N=N2+1
   14 X(N)=SR1*X(N)+CA*(2.*X(N-1)+X(N+NV1)+X(N-NV1))
      N=NA*NV1
      X(N )=SR1*X(N )+CA*(2.*X(N -1)+X(N +NV1)+X(N -NV1))
      IF(ITR.EQ.1.AND.MD4.EQ.1) CALL CROSS(-1,X,Y,Y1,P,RES,H,XKP,NV,NA1,
     XNA2,NC,NV1)
C*** CROSSOVER TO REGION R
      CALL FLIP(X,Y,P, 1,RES,XKP,H,NC,NA1,NV1,UINF,MD4,ITR)
      RETURN
      END



      SUBROUTINE READY(X,Y,ZB,ZS,NH1,NV1,NTOT1,X0)
C*** INTERPOLATE SOLUTION ALONG BOUNDARY FOR MESH REFINEMENT  BY A
C     FACTOR OF 2
      DIMENSION X(1),Y(1),ZB(1),ZS(1)
      COMPLEX ZS,ZB
      DO 50 N=1,NTOT1
      X(N)=0.
   50 Y(N)=0.
      DO 51 L=1,NH1,2
      N1=1+(L-1)*NV1
      X(N1)=REAL(ZB(1+L/2))
   51 Y(N1)=AIMAG(ZB(1+L/2))
      DO 52 L=1,NV1,2
      N1=NTOT1-L+NV1
      X(N1)=REAL(ZS(1+L/2))
   52 Y(N1)=AIMAG(ZS(1+L/2))
      X0=X(1)
      DO 53 L=1,NV1
   53 X(L)=X0
      DO 40 L=5,NH1,2
      N1=NV1*(L-2)+1
      X(N1)=.125*(-X(N1-3*NV1)+6.*X(N1-NV1)+3.*X(N1+NV1))
   40 Y(N1)=.125*(-Y(N1-3*NV1)+6.*Y(N1-NV1)+3.*Y(N1+NV1))
      DO 41 L=5,NV1,2
      N1=NTOT1+L-3-NV1
      X(N1)=.125*(3.*X(N1-1)+6.*X(N1+1)-X(N1+3))
   41 Y(N1)=.125*(3.*Y(N1-1)+6.*Y(N1+1)-Y(N1+3))
      N1=NV1+1
      X(N1)=.5*(X(N1+NV1)+X( N1-NV1))
      Y(N1)=.5*(Y(N1+NV1)+Y( N1-NV1))
      N1=NTOT1-1
      X(N1)=X(NTOT1)
      Y(N1)=.5*Y(NTOT1-2)
      RETURN
      END
```

PAGE NO. 6

```
      SUBROUTINE SPEW(NSPEW)
C*** DIVULGE ANSWERS
C  NSPEW=1 INITIAL DATA                  6 ITERATION DATA
C        2 HEADER FOR ITERATION DATA     7 CONVERGENCE DATA
C        3 FIXED BOUNDARY DATA           8 NODAL LINES
C        4 FREE BOUNDARY DATA            9 PSI DERIV ALONG FREE BOUNDARY
C        5 DIVERGENCE DATA              10 DRAG CALCULATION
      COMMON/B1/ADV,BDV,CDV,X0,NV,NH,NV1,NH1,NTOT,NC,SR1,CA,SRI,H,NIT
      COMMON/B2/XKL,XKLP,XK,XKP,E,EP,Q,QP,IS1,IS2
     1,MD1,MD2,MD3,MD4,AVG1,AVG2,AMAX,BMAX,CMAX,MAXA,MAXB,MAXC,B1,B2,B3,
     2SR,L,ERLIM,HLENGH,UINF,IP,NE,NEP,NL,EPS,ZB(225),ZS(100),
     3UD(225),VD(225),PSIV(225),CON(50),  X( 2000) ,Y( 2000),PSI( 2000)
      DIMENSION NS(100)
      COMPLEX ZB,ZS,Z1,Z2,EZ,UD,VD
      GO TO (1,2,3,4,5,6,7,8,9,26),NSPEW
    1 PRINT 10,XKL,SR,CON(4),H,B1,CON(1),XKLP,NIT,NH1,B2,CON(2),XK,ERLIM
     1,NV1,B3,CON(3),XKP,IP,NTOT,NE,E,MD1,HLENGH,NEP,EP,MD2,UINF,EPS,Q
     2,MD3,NC,QP,MD4,NL
   10 FORMAT(1H1, 9X,*KL*,F12.8,4X,*RELAXATION FACTOR*,2F7.4, 7X,
     1*MESH SIZE*,F10.6,5X,*CONVERGENCE  B1*,2F7.4/5X,*KLPRIME*,F12.8,3X
     2,*MAXIMUM ITERATIONS*,I14, 7X,*HORIZ PTS*,I10,9X,*FACTORS  B2*,
     32F7.4/11X,*K*,F12.8,10X,*ERROR LIMIT*,F14.2, 8X,*VERT PTS*,I1
     4,18X,*B3*,2F7.4/6X,*KPRIME*,F12.8,19X,*IP*,I14,1X,
     5*TOTAL EQUATIONS*,I10,4X,*PTS IN*,8X,*NE*,I7/11X,*E*,F12.8,8X,*INP
     6UT SET MD1*,I14,4X,*CAVITY LENGH*,F10.6,4X,*EXTRAP   NEPRIME*,I7/
     76X,*EPRIME*,F12.8,18X,*MD2*,I14,1X,*VEL AT INFINITY*,F10.6,4X,*EXT
     8RAP AT    EPS*,F7.2/11X,*Q*,F12.8,18X,*MD3*,I14,30X,*INTERFACE
     9 NC*,I7/6X,*QPRIME*,F12.8,18X,*MD4*,I14,32X,*L-SHIFT*,5X,*NL*,I7)
      RETURN
    2 PRINT 13
   13 FORMAT(///5X,*ITERATION DATA*//2X,*ITER     AMAX-INDEX     BMAX-IN
     1DEX      CMAX-INDEX      MDPT    SEPPT     1/Q0SQ     1/Q1SQ     1/Q2SQ
     2 SLOPE1   SLOPE2     RES-X0         X0*/)
      RETURN
    6 Z1=CMPLX(AIMAG(ZB(  1)),AIMAG(ZB(NH1)))
      PRINT 14,I,AMAX,MAXA,BMAX,MAXB,CMAX,MAXC,Z1,AVG1,CON(1),CON(3)
     1 ,CON(2),CON(4),AVG2,X0
   14 FORMAT(1X,I5,3(E11.2,I4),F9.5,F8.5,3F10.4,2F8.4,2F10.5)
      RETURN
    3 PRINT 25,I,(ZS(L),L=1,NV1)
   25 FORMAT(//5X,*FIXED BOUNDARY AT ITERATION*,I5//(7(F10.6,F9.6)))
      PRINT 15, ((UD(L),VD(L)),L=1,NV1)
   15 FORMAT(//5X,*FIXED BOUNDARY DERIVATIVES  XU/YU/XV/YV*,//(4(2X,4F8.
     X5)))
      RETURN
    4 PRINT 18,I,(ZB(L),L=1,NH1)
   18 FORMAT(//5X,*FREE BOUNDARY AT ITERATION*,I5//(7(F10.6,F9.6)))
      PRINT 17, ((UD(L),VD(L)),L=1,NH1)
   17 FORMAT(//5X,*FREE BOUNDARY DERIVATIVES  XU/YU/XV/YV*,//(4(2X,4F8.5
     X)))
      RETURN
    5 PRINT 19, I
   19 FORMAT(////10X,*DIVERGENCE AT ITERATION*,I5)
      RETURN
    7 PRINT 20,ERLIM
```

PAGE NO. 7

```
   20 FORMAT(//10X,*ERROR IS BELOW*,E10.1,//)
      GO TO 8
    8 PRINT 85
      N1=2+NV1
      N2=NC+1+NV1
      DO 81 L=2,NH
      DO 82 N=N1,N2
      N3=N-N1+1
      XU=(X(N+1)-X(N-1))**2+(Y(N+1)-Y(N-1))**2-(X(N+NV1)-X(N-NV1))**2
     1-(Y(N+NV1)-Y(N-NV1))**2
      IF(XU.GT.0) NS(N3)=1
      IF(XU.LE.0) NS(N3)=0
   82 CONTINUE
      PRINT 83,(NS(K),K=1,N3)
      N1=N1+NV1
   81 N2=MIN0(NC+L*(NV1+1),L*NV1+NV)
   85 FORMAT(//10X,7AHLOCATION OF NODAL LINES OF (XV**2+YV**2-XU**2-YU**
     X2)   1  IF (+)     0 IF (-)    //)
   83 FORMAT(5X,100I1)
      RETURN
    9 PRINT 16,(PSIV(L),L=1,NH1)
   16 FORMAT(////10X,*PSIV ALONG FREE BOUNDARY*//(1X,15F9.6))
      RETURN
   26 CALL DERIV(UD,VD,PSIV,X,Y,PSI,ZB,ZS,3)
      PRINT 27,(PSIV(L),L=1,NV1)
   27 FORMAT(//10X,*PSIU ALONG FIXED BOUNDARY*//(1X,15F9.6))
      CON(1)=REAL(ZB(NH1))
      CON(2)=AIMAG(ZB(1))
      CON(3)=AIMAG(ZB(NH1))
      CON(4)=SQRT(1./AVG1)
      SGEX=2.*XKLP/(1.-XKLP)
      SGCMP=1./AVG1/UINF**2-1.
      CDEX=2.*(EP*XKL**2+XKP)/(XKLP**2*EP+XKL**2*XKP)
      A=0.
      B=0.
      DO 21 L=3,NV,2
   21 A=A+PSIV(L)**2/AIMAG(VD(L))/AIMAG(ZS(L))**MD4
      DO 22 L=2,NV,2
   22 B=B+PSIV(L)**2/AIMAG(VD(L))/AIMAG(ZS(L))**MD4
      CDCMP=1.+(1.+MD4)*AVG1/AIMAG(ZB(NH1))**(1+MD4)*(H/3.*(4.*B+2.*A))
      PRINT 24,CON(1),CON(2),CON(3),UINF,CON(4),SGEX,SGCMP,CDEX,CDCMP
   24 FORMAT(//10X,*DRAG DATA*//16X,*SEPARATION POINT  X*,F10.6,17X,*CAV
     XITY HEIGHT*,F10.6/34X,*Y*,F10.6,13X,*SPEED AT INFINITY*,F10.6/16X,
     X*FREE BOUNDARY SPEED*,F10.6//5X,*EXACT VALUES*,13X,*SIGMA*,F10.6,3
     XX,*COMPUTED VALUES*,7X,*SIGMA*,F10.6/3X,*(PLANE CASE ONLY)   CD/(1
     X+SIGMA)*,F10.6,18X,*CD/(1+SIGMA)*,F10.6)
      RETURN
      END
```

PAGE NO. 8

```
      SUBROUTINE CROSS(K,X,Y,Y1,P,RES,H,XKP,NV,NA1,NA2,NC,NV1)
C*** SET Y VALUES IN REGION R1 AND PSI(STAR) ALONG INTERFACE
C    AXIALLY SYMMETRIC CASE ONLY
      DIMENSION X(1),Y(1),P(1),Y1(1)
      COMPLEX Z1,Z2
      N1=NC
      DO 1 L=1,NA1
      N2=N1+1
      IF(L.EQ.NA1) N2=N1
      DO 2 N=N1,N2
      Z1=1./(CMPLX(X(N)-X(1) ,Y(N))+RES/CMPLX((L-1)*H,(NC-2.+L+N-N1)*H-X
     1KP))
      IF(K.EQ.1) Y1(N)=AIMAG(Z1)
    2 P(N)=P(N)*SQRT(REAL(Z1*CONJG(Z1)))**K
    1 N1=N1+NV+2
      IF(K.EQ.-1) RETURN
      N1=NC+2
      N2=NV1
      DO 3  L=1,NA2
      DO 4  N=N1,N2
      IF(N.EQ.NV1) GO TO 4
      Y1(N)=AIMAG(1./(CMPLX(X(N)-X(1) ,Y(N))+RES/CMPLX((L-1)*H,(N-N2+NV)
     1*H-XKP)))
    4 CONTINUE
      N1=N1+NV1+1
    3 N2=N2+NV1
      Y1(NV1)=0.
      RETURN
      END
```

```
      SUBROUTINE EXTRAP(FB,XS,N,H,NV1,UD,PSIV,A0,A1,M,MD4,Z)
C*** EXTRAPOLATION FOR 1/Q1SQ (M=2) AND 1/Q2SQ (M=1)
      DIMENSION UD(1),PSIV(1),Z(1)
      COMPLEX UD,Z
      FDET(Z1,Z2,Z3,Z4)=Z1*Z4-Z2*Z3
      A=0. $ B=0. $ C=0. $ D=0.
      DO 1 L=1,N
      GO TO (3,2),M
    2 K=NV1-L
      A=A-L*H
      D=D+REAL(UD(K)*CONJG(UD(K)))/PSIV(K)**2*AIMAG(Z(K))**(2*MD4)*(-H*L
     1 )
      GO TO 4
    3 K=L+1
      A=A+L*H
      D=D+REAL(UD(K)*CONJG(UD(K)))/PSIV(K)**2*AIMAG(Z(K))**(2*MD4)*(H*L)
    4 C=C+REAL(UD(K)*CONJG(UD(K)))/PSIV(K)**2*AIMAG(Z(K))**(2*MD4)
    1 B=B+(L*H)**2
      DET=FDET(FLOAT(N),A,A,B)
      A0=FDET(C,A,D,B)/DET
      A1=FDET(FLOAT(N),C,A,D)/DET
      FB=A0
      RETURN
      END
```



```
      FUNCTION FF1(U,E,XK,Q)
C*** FORMULA 905.01 PAGE 300 REFERENCE (4)
      PI=3.14159265358979
      A=PI*U/XK  $SUM=0.  $P=1.  $P2=1.  $Q2=Q**2
      DO 1 L=1,100
      P=P*Q
      P2=P2*Q2
      R=P/(1.-P2)
      IF(R.LE. 1.E-12) GO TO 2
      SUM=SUM+R*SIN(L*A)
    2 FF1=(2.*PI*SUM +E*U)/XK
      RETURN
      END
```

```
      FUNCTION FF(DPSI,DKSQ)
C*** FORMULA 903.00 PAGE 299 REFERENCE(4)
      DT=DPSI $ DFK=DT $ CF=1.
      DO 1 L=1,450
      CF=(L-.5)/L*CF
      DT=((2.*L-1.)*DT-SIN(DPSI)**(2*L-1)*COS(DPSI))/(2.*L)
    1 DFK=DFK+CF*DT*(-DKSQ)**L
      FF=DFK
      RETURN
      END
```

```
      FUNCTION SNF(W,Q,XK,XKC)
C*** FORMULA 908.01 PAGE 303 REFERENCE (4)
      PI=3.14159265358979
      A=PI*W*.5/XK
      [illegible]=1+24/ALOG(1./Q)
      SNF=SIN(A)/(1.-Q)
      DO 1 I=1,[illegible]
    1 SNF=SNF+[illegible]**I*SIN((2*I+1)*A)/(1.-Q**(2*I+1))
      SNF=SNF*SQRT(Q)*2.*PI/(XK*XKC)
      RETURN
      END
```

```
      FUNCTION FX1(Q)
C*** FORMULA 900.04 PAGE 297 REFERENCE (4)
      SUM=1.
      DO 1 L=1,20
    1 SUM=SUM+4.*Q**L/(1.+Q**(2*L))
      FX1=3.14159265358979*[illegible]  /2.
      RETURN
      END
```

```
      FUNCTION FXKL(XK,Q)
C*** EXAMPLE 3 PAGE 474 REFERENCE (16)
      SUM=0.
      DO 1 I=1,100
      S1=Q**(I*(I-1))
      SUM=SUM+S1
      IF(S1 .LE. 1.E-13) GO TO 2
    1 CONTINUE
    2 FXKL=3.14159265358979/XK*2.*SQRT(Q)*SUM**2
      RETURN
      END
```

KL	.93064809	RELAXATION FACTOR	1.7611	1.0000	MESH SIZE	.035645	CONVERGENCE	B1	.2170	1.6000					
KLPRIME	.36591545	MAXIMUM ITERATIONS		3000	HORIZ PTS	19	FACTORS	B2	.0543	.4000					
K	2.44162065	ERROR LIMIT		1.00E-06	VERT PTS	13		B3	.0543	.4000					
KPRIME	1.62774710	IP		1	TOTAL EQUATIONS	247	PTS IN	NE	13						
E	1.13140818	INPUT SET MD1		2	CAVITY LENGH	.864440	EXTRAP	NEPRIME	2						
EPRIME	1.51661566	MD2		1	VEL AT INFINITY	.481337	EXTRAP WT	EPS	.02						
Q	.12314471	MD3		3			INTERFACE	NC	4						
QPRIME	.00896329	MD4		1			L-SHIFT	NL	5						

FIXED BOUNDARY AT ITERATION 0

.864440	.268662	.864440	.257613	.864440	.253466	.864440	.245864	.864440	.234337	.864440	.218542	.864440	.198249		
.864440	.173627	.864440	.144765	.864440	.112185	.864440	.076583	.864440	.038844	.864440	0.000000				

FIXED BOUNDARY DERIVATIVES XU/YU/XV/YV

.00077	-.00845	0.00000	-.00921	-.02023	-.00012	0.00000	-.01989	-.04320	-.00026	0.00000	-.04331	-.06998	-.00043	0.00000	-.07051
-.09979	-.00056	0.00000	-.10071	-.13158	-.00071	0.00000	-.13284	-.16402	-.00084	0.00000	-.16556	-.19557	-.00091	0.00000	-.19733
-.22457	-.00090	0.00000	-.22648	-.24932	-.00080	0.00000	-.25132	-.26829	-.00060	0.00000	-.27034	-.28022	-.00032	0.00000	-.28229
-.28429	0.00000	0.00000	-.28637												

FREE BOUNDARY AT ITERATION 0

0.000000	.061174	.125469	.195064	.266448	.336004	.359026	.481760	.460302	.403435	.548573	.442309	.623285	.419652		
.684822	.556605	.734220	.674095	.772868	.852831	.802380	.333313	.824236	.815862	.839887	.800665	.850611	.287813		
.857520	.277334	.861573	.269263	.863602	.263457	.864336	.260009	.864440	.258862						

FREE BOUNDARY DERIVATIVES XU/YU/XV/YV

.92498	0.00000	0.00000	.91758	.90843	-.04485	.04514	.90110	.86041	-.08590	.08625	.85384	.78828	-.12006	.12010	.78168
.69868	-.14542	.14481	.69278	.60076	-.16139	.15992	.59582	.50222	-.16048	.16017	.49843	.40892	-.16794	.16499	.40634
.32462	-.13135	.13084	.32320	.25124	-.15032	.14695	.25080	.18427	-.13027	.13006	.18957	.13825	-.12054	.11747	.13907
.09722	-.10339	.10093	.09834	.06499	-.08600	.08398	.06625	.04041	-.06052	.06095	.04168	.02242	-.05115	.05000	.02362
.01018	-.03396	.03322	.01125	.00309	-.01694	.01657	.00499	.00077	-.00846	0.00000	-.00921				

PSIV ALONG FREE BOUNDARY

.370650	.362515	.339381	.304654	.262994	.219193	.177205	.139645	.110774	.086199	.061254	.045348	.030197	.023964	.016919	
.011457	.007081	.003379	0.000000												

ITERATION DATA

ITER	AMAX-INDEX		BMAX-INDEX		CMAX-INDEX		MDPT	SEPPT	1/Q1SQ	1/Q1SQ	1/Q2SQ	SLOPE1	SLOPE2	RES-X0	X0
50	5.30E-02	19	-3.62E-03	18	-4.09E-02	2	.49458	.25640	1.6014	1.5867	2.3471	-.0075	4.3194	.00011	-.00600
100	3.22E-02	19	-7.53E-03	18	-2.51E-02	2	.49222	.25455	1.6045	1.5954	2.1515	-.0061	4.6894	.00017	-.00607
150	2.00E-02	19	-5.36E-03	18	-1.58E-02	2	.49100	.25344	1.6059	1.5963	1.9796	-.0043	5.0158	.00012	-.00464

200	1.27E-02	18	-3.71E-03	18	-1.02E-02	2	.49029	.25272	1.6038	1.6016	1.8590	-.0029	5.2387	.00008	-.01073
250	8.34E-03	18	-2.56E-03	18	-6.83E-03	2	.48983	.25225	1.6014	1.6039	1.7784	-.0020	5.3844	.00006	-.01148
300	5.99E-03	18	-1.77E-03	18	-4.63E-03	2	.48952	.25195	1.6013	1.6054	1.7248	-.0014	5.4799	.00004	-.01199
350	3.81E-03	18	-1.23E-03	18	-3.15E-03	2	.48931	.25175	1.6008	1.6064	1.6887	-.0009	5.5434	.00003	-.01235
400	2.62E-03	18	-8.59E-04	18	-2.20E-03	2	.48916	.25160	1.6002	1.6071	1.6642	-.0007	5.5861	.00002	-.01259
450	1.82E-03	18	-6.02E-04	18	-1.54E-03	2	.48906	.25150	1.6004	1.6076	1.6474	-.0005	5.6152	.00001	-.01276
500	1.27E-03	18	-4.22E-04	18	-1.07E-03	2	.48898	.25143	1.6003	1.6079	1.6358	-.0003	5.6353	.00001	-.01288
550	8.84E-04	18	-2.97E-04	18	-7.53E-04	2	.48893	.25139	1.6001	1.6081	1.6277	-.0002	5.6492	.00001	-.01296
600	6.24E-04	18	-2.09E-04	18	-5.29E-04	2	.48890	.25135	1.6000	1.6083	1.6221	-.0002	5.6589	.00000	-.01302
650	4.39E-04	18	-1.47E-04	18	-3.72E-04	2	.48887	.25133	1.6000	1.6084	1.6181	-.0001	5.6657	.00000	-.01306
700	3.09E-04	18	-1.04E-04	18	-2.62E-04	2	.48885	.25131	1.6000	1.6085	1.6153	-.0001	5.6704	.00000	-.01309
750	2.17E-04	18	-7.31E-05	18	-1.85E-04	2	.48884	.25130	1.6001	1.6085	1.6134	-.0001	5.6738	.00000	-.01310
800	1.53E-04	18	-5.15E-05	18	-1.30E-04	2	.48883	.25129	1.6001	1.6086	1.6120	-.0000	5.6761	.00000	-.01312
850	1.07E-04	18	-3.64E-05	18	-9.19E-05	2	.48883	.25128	1.6001	1.6086	1.6110	-.0000	5.6778	.00000	-.01313
900	7.56E-05	18	-2.57E-05	18	-6.49E-05	2	.48882	.25128	1.6001	1.6086	1.6103	-.0000	5.6789	.00000	-.01314
950	5.33E-05	18	-1.81E-05	18	-4.58E-05	2	.48882	.25128	1.6001	1.6087	1.6098	-.0000	5.6798	.00000	-.01314
1000	3.74E-05	18	-1.28E-05	18	-3.23E-05	2	.48882	.25128	1.6001	1.6087	1.6095	-.0000	5.6803	.00000	-.01314
1050	2.63E-05	18	-9.02E-06	18	-2.28E-05	2	.48881	.25127	1.6001	1.6087	1.6093	-.0000	5.6808	.00000	-.01315
1100	1.84E-05	18	-6.36E-06	18	-1.61E-05	2	.48881	.25127	1.6001	1.6087	1.6091	-.0000	5.6810	.00000	-.01315
1150	1.33E-05	18	-4.49E-06	18	-1.14E-05	2	.48881	.25127	1.6001	1.6087	1.6090	-.0000	5.6812	.00000	-.01315
1200	9.41E-06	18	-3.17E-06	18	-8.01E-06	2	.48881	.25127	1.6001	1.6087	1.6089	-.0000	5.6814	.00000	-.01315
1250	6.64E-06	18	-2.24E-06	18	-5.65E-06	2	.48881	.25127	1.6001	1.6087	1.6088	-.0000	5.6815	.00000	-.01315
1300	4.69E-06	18	-1.58E-06	18	-3.99E-06	2	.48881	.25127	1.6001	1.6087	1.6088	-.0000	5.6816	.00000	-.01315
1350	3.31E-06	18	-1.11E-06	18	-2.82E-06	2	.48881	.25127	1.6001	1.6087	1.6088	-.0000	5.6816	.00000	-.01315
1400	2.34E-06	18	-7.87E-07	18	-1.99E-06	2	.48881	.25127	1.6001	1.6087	1.6087	-.0000	5.6817	.00000	-.01315
1450	1.65E-06	18	-5.55E-07	18	-1.40E-06	2	.48881	.25127	1.6001	1.6087	1.6087	-.0000	5.6817	.00000	-.01315
1500	1.16E-06	18	-3.92E-07	18	-9.91E-07	2	.48881	.25127	1.6001	1.6087	1.6087	-.0000	5.6817	.00000	-.01315

ERROR IS BELOW 1.0E-06

1522	9.95E-07	18	0.	18	0.	2	.48881	.25127	1.6001	1.6087	1.6087	-.0000	5.6817	.00000	-.01315

FREE BOUNDARY AT ITERATION 1522

-.013153	.488810	.113080	.485571	.234984	.476202	.348731	.461663	.451379	.443306	.541103	.422538	.617214	.400663
.679995	.378748	.730437	.357606	.769942	.337814	.800087	.319757	.822448	.303675	.838492	.289699	.849531	.277841
.856702	.268264	.860987	.260808	.863229	.255502	.864164	.252341	.864440	.251271				

FREE BOUNDARY DERIVATIVES XU/YU/XV/YV

.93061	0.00000	.00000	.92929	.91465	-.04648	.04642	.91357	.86863	-.08010	.08806	.86822	.79765	-.12125	.12134	.79822
.70910	-.14424	.14458	.71077	.61128	-.15719	.15788	.61399	.51197	-.16141	.16252	.51548	.41735	-.15871	.16022	.42133
.33155	-.13089	.13275	.33565	.25674	-.13991	.14163	.26063	.19324	-.12584	.12810	.19701	.14156	-.11080	.11306	.14446
.09983	-.08504	.09720	.10210	.06712	-.07901	.08096	.06878	.04223	-.06297	.06460	.04332	.02406	-.04704	.04828	.02469
.01171	-.03121	.03205	.01203	.00446	-.01560	.01591	.00453	.00203	-.00749	.00800	-.00789				

FIXED BOUNDARY AT ITERATION 1522

.864440	.251271	.864440	.250200	.864440	.246380	.864440	.239243	.864440	.228295	.864440	.213106	.864440	.193651
.864440	.169745	.864440	.141667	.864440	.109874	.864440	.075050	.864440	.038081	.864440	0.000000		

```
FIXED BOUNDARY DERIVATIVES  XU/YU/XV/YV

 .00203 -.[illegible] .[illegible] -.00749   -.01841  .00000  .00000 -.01803   -.04[illegible]  .[illegible] [illegible] -.04039   -.06721  .0000[illegible] 0.00000 -.06666
-.09665  .[illegible]  .[illegible] -.09612   -.12813  .00000 0.00000 -.12773   -.16[illegible]  .[illegible] [illegible] -.16005   -.19166  .00000 0.00000 -.19162
-.22050  .[illegible]  .[illegible] -.22059   -.24515  .00000 0.00000 -.24556   -.26[illegible]  .[illegible] [illegible] -.26463   -.27590  .00000 0.00000 -.27664
-.27995 0.[illegible] [illegible] -.28074


      PSIV ALONG FREE BOUNDARY

 .358142  .[illegible]  .327647  .293865  .255515  .211149  .170739  .134607  .[illegible]  .[illegible]  .059243  .043922  .032199  .023274  .016452
 .011151  .[illegible]  .003292 0.000000

      PSIU ALONG FIXED BOUNDARY

0.000000 -.002966 -.[illegible]673 -.007787 -.009108 -.009[illegible] -.008968 -.107622 -.[illegible] -.[illegible] -.001763 -.000464 0.000000

      DRAG DATA

            SEPARATION POINT  X   .864440                   CAVITY HEIGHT    .[illegible]
                              Y   .251271                 SPEED AT INFINITY  .[illegible]
            FREE BOUNDARY SPEED   .788430

  EXACT VALUES              SIGMA  1.154154   COMPUTED VALUES      SIGMA    .[illegible]
 (PLANE CASE ONLY)      CD/(1+SIGMA)  .888426               CD/(1+SIGMA)    .[illegible]

      LOCATION OF NODAL LINES OF (XV**2+YV**2-XU**2-YU**2)   1  IF (+)    [illegible] IF (-)

 1111
 11111
 111111
 1111111
 1111110
 1111100[illegible]
 1111000[illegible]
 1110000[illegible]
 1100000[illegible]
 0100000[illegible]
 1100000[illegible]
 1100000[illegible]
 1110000[illegible]
 1110000[illegible]
 1110000[illegible]
 1111000[illegible]
 1111000[illegible]
```

N.Y.U. Courant Institute of
Mathematical Sciences
251 Mercer St.
New York, N. Y. 10012